Changes in channel geometry through the Holocene in the Le Sueur River, south-central Minnesota, USA

A Thesis
SUBMITTED TO THE FACULTY OF
UNIVERSITY OF MINNESOTA
BY

Courtney Ann Targos

IN PARTIAL FULFILLMENT OF THE REQUIREMENTS
FOR THE DEGREE OF
MASTER OF SCIENCE

Dr. Karen Gran

March 2017

Acknowledgements

I would like to thank my mother, Kath, and my Stepdad, Walter, for always believing in me. My brothers are pretty cool too, I suppose. I would like to thank my advisor, Dr. Karen Gran for all of her brilliant ideas and support. I would also like to thank the National Science Foundation (NSF) grant EAR-1209402 for funding my project. I would also like to thank the Department of Earth and Environmental Sciences at the University of Minnesota Duluth for funding parts of my project. And, thank the Minnesota Geological Survey (MGS) for lending me the Giddings equipment needed to complete my fieldwork. I would also like to thank Harry Jol and his student, Sean Morrison, for their assistance in processing GPR profiles. Finally, I would like to thank Aaron Knowlton and Nate Mitchell for assistance in the field.

Dedication

This thesis is dedicated to my family, friends, partner, and my wonderful advisor without whom this thesis would have been very difficult.

Abstract

Paleochannels preserved on terraces via meander cutoffs during an incisional period record the channel geometry and thus discharge at distinct points in time throughout a river's history. We measured paleochannel geometry on terraces throughout the Le Sueur River in south-central Minnesota, to track how channel geometry has changed over the last 13,400 years. A rapid drop in base level 13,400 yr B.P. triggered knickpoint migration and valley incision that is ongoing today. Since the 1800's, the area has developed rapidly with an increase in agriculture and associated drainage, directly impacting river discharge by increasing water input to the river. Five paleochannels were identified on terraces along the Le Sueur River from 1m-resolution lidar data. Ground Penetrating Radar (GPR) was used to obtain a subsurface image across paleomeanders to estimate the geometry of paleochannels. Paleochannel geometry and estimated discharge were then compared to modern conditions to assess how much change has occurred. Three lines were run across each paleochannel perpendicular to the historic water flow. Each of the 15 lines were processed using the EKKO Project 2 software supplied by Sensors and Software to sharpen the images, making it easier to identify the paleochannel geometry. Paleodischarge was determined using the Law of the Wall and Manning's Equation, using modern slope and roughness conditions. OSL samples were collected from overbank deposits on terraces to determine the time of channel abandonment, and supplemented with terrace ages obtained from a numerical model of valley incision. Paleodischarge coupled with depositional ages provide a history of flow conditions on the Le Sueur River.

Results show an increase in channel widths from the time paleochannels were occupied to modern channel dimensions from an average of 20 meters to 35 meters. The change was not constant through time, as all paleochannels analyzed on terraces had similar-sized channels. The best way to determine paleogeometry was using the 'best interpretation' of GPR data couple with coring data; and paleodischarge was best estimated using Manning's equation with an *n* value of 0.035. Results show an increase in discharge compared to paleochannels of a factor of two. Uncertainty estimates in GPR-based paleogeometry can change paleodischarge calculations by 50 %. Incremental flood frequency analyses, based on data obtained from the Red Jacket stream gage at the outlet of the Le Sueur, suggest a 1.5- and 2-year flood of 102 m^3/s and 154 m^3/s, respectively, which is comparable to estimations of bankfull based on current channel geometry at the Red Jacket gage, validating the methodology. Problems associated with paleogeometry estimations are primarily due to meander bend preservation in the subsurface, challenging GPR interpretation. The increase in channel geometry and discharge implies that the increase in flow associated with drainage and climate change since the area's development has greatly impacted the Le Sueur River. This resulted in a change in channel morphometry through increased erosion along the bluffs and banks, widening channels. This increase in erosion has directly impacted the amount of sediment delivered to the rivers from banks and bluffs, increasing the fine sediment load in this turbidity-impaired river system.

Table of Contents

List of Tables

List of Figures

Section 1: Introduction

The Minnesota River Basin (MRB) is located in south-central Minnesota with an area of 43,400 km^2 (Figure 1.1). Changes to this landscape have been occurring over two very different timescales as a response to long-term (Holocene base level drop) and short-term (anthropogenic) perturbations. The first timescale marks changes throughout the Holocene and late Pleistocene due to a drop in base-level. The second timescale describes changes since settlement began in the 1800's due to anthropogenic factors, including climate and land use changes. It is important to understand the longer timescale changes within the watershed to provide context for the analysis of basin response to anthropogenic changes.

The Minnesota River Valley (MRV) formed at the end of the Wisconsinan glaciation in the late Pleistocene when glacial Lake Agassiz drained through its southern outlet (Clayton and Moran, 1982). Prior to this drainage, Minnesota experienced several cycles of glaciation that blanketed south-central Minnesota with glacial till and outwash (Clayton and Moran, 1982). The carving of the Minnesota River Valley (13.5 ka BP) resulted in a drop in the regional base-level felt by tributaries to the Minnesota River (Belmont et al., 2011**b**). Three major tributaries of the Minnesota River are found within the Greater Blue Earth River (GBER) basin, which occupies an area of 9,169 km^2 (MPCA, 2014). These tributaries are the Le Sueur River, Watonwan River, and Blue Earth River. Due to the long-term perturbation (drop in base-level), the rivers in the GBER watershed have knickpoints that have migrated upstream, approximately 40 km, 35 km, and 65 km for the Le Sueur River, Watonwan River, and Blue Earth River,

respectively, as a direct result of the base-level drop (Bevis, 2015). Below the knickpoint, the "knickzone" has higher valley walls and steeper bed gradients, resulting in the creation of bluffs and ravines (Belmont et al., 2011b). The valley walls within the GBER are composed of competent glacial till, primarily the New Ulm Formation, which is clay-rich and dense (Jennings, 2007). Valley incision and creation of bluffs and ravines in the watershed are a direct response to the long-term perturbation of base-level fall.

Perturbations have also occurred over a short-time scale. Land use has changed dramatically over the course of 200 years in the MRB. Originally covered by 85% prairie and wet prairie, the area is currently comprised of greater than 90% agriculture (NLCD, 2011). Many of these agricultural lands are drained by surface drainage and sub-surface tile drainage, an agricultural practice that has been increasing since its introduction in the early 1900's (Minnesota Historic Farms Study; Schottler et al., 2013). With the increase in agriculture, there has been a similar trend in tile drainage installation. This practice routes water more directly to the rivers, decreasing the erosion of the uplands via overland flow while increasing the total volume of water in rivers (Blann et al., 2009).

Over the last 200 years, the amount of sediment moving through the Minnesota River system and being deposited in Lake Pepin has increased ten-fold (Engstrom et al., 2009). It has been determined that most sediment is coming from near-channel sources (bluffs and banks) from fluvial scour, oversteepening the toe of bluffs and scouring banks (Belmont et al., 2011). At the same time, there has been a documented increase in summer peak flows due to rainfall events, high flow days, and base flow during the winter and summer in the last 90 years (Novotny and Stefan, 2007). Several factors have

caused the increase in discharge, including settlement of the area and land use changes, climate change, and the introduction of tile drainage (Schottler et al., 2013). The increase in discharge has resulted in more bank erosion in the rivers and has also increased channel width by 10-40% since 1940 (Schottler et al., 2013). Changes in channel width and sediment loading documented over the past 70 years (1940-2009) lead to the question: what was the effective discharge prior to settlement of the basin?

The effective discharge of a river, or the discharge that moves the most sediment over time sets the geometry of the river channel. Generally, the effective discharge is represented by the bankfull discharge which is often a 1.5 to 2-year flood. By examining geometry of paleochannels, we can measure how the effective discharge has changed over time throughout the Holocene and late Pleistocene.

A paleochannel is an old, abandoned river channel. Incision, avulsion, and migration can lead to meander bend preservation, with incision and avulsion being the best methods of preservation. Migration is a form of channel movement, however, this process may erase the signature of the previous channel as it moves across the floodplain, reworking sediments. In incisional environments, channel geometry is often preserved. Once the meander bend is cut-off, it would normally fill in with overbank deposits through time. This infilling should preserve the channel form, allowing it to be studied.

In the Greater Blue Earth River (GBER) basin, the drop in base-level and ensuing knickpoint migration led to the formation of hundreds of terraces, many of which contain stranded paleochannels preserving the geometry of the channel at the time it was active. Paleochannel geometry recorded on Holocene-age terraces may even record large climate

excursions like the mid-Holocene dry period (MHDP) and the Little Ice Age (LIA), which occurred 4 ka to 9 ka years ago and from 1650 to 1850 AD, respectively. This project focuses on the Le Sueur River, one of the 3 tributaries in the GBER basin, because there has already been work done on the excavation history (Gran et al., 2013), and aims to add to the discharge history. The discharge history is likely similar in the Maple and Cobb Rivers, as well as in the neighboring Watonwan and Blue Earth Rivers.

The goal of this thesis is to construct a paleodischarge history for the Le Sueur River investigating the last 13,400 years, in which discharge changes are expected from drainage network expansion and potentially from climate excursions occurring during the Holocene. Estimations of paleochannel geometry were completed on a series of terraces in the Le Sueur River that exhibit well-preserved stranded meander cutoffs. Samples collected in paleochannels were dated with OSL (optically-stimulated luminescence) to determine depositional ages of sediments. Coupling both the dimensions of paleochannels and depositional ages within the LS basin allowed the construction of a Holocene-scale history of discharge in the Le Sueur River. The effective discharge that formed each paleochannel was compared to current bankfull discharge measurements, thus reconstructing a portion of the paleodischarge history of the Le Sueur River. Flood frequency analyses conducted throughout the last century provide context for modern and pre-settlement estimates of effective discharge calculations.

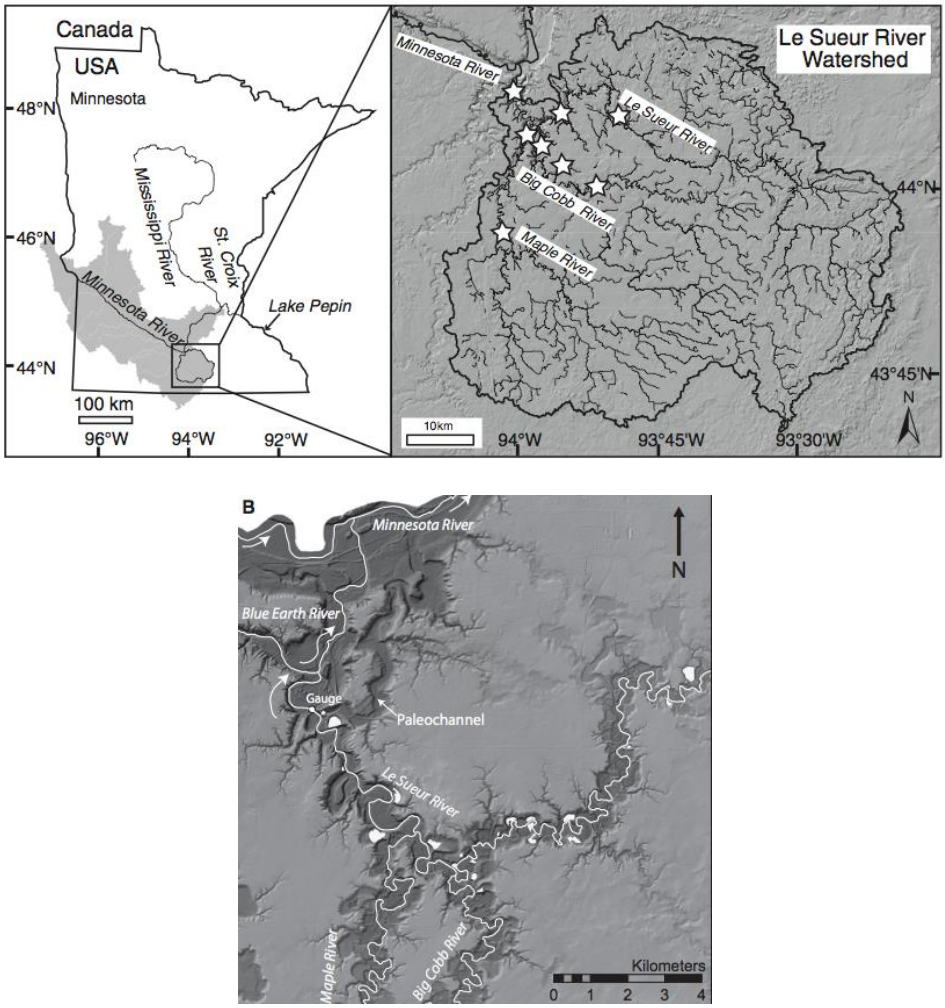

Figure 1.1. Map showing location of Le Sueur River within the Minnesota River Basin. Within the Le Sueur River watershed are the Maple and Cobb Rivers, tributaries to the Le Sueur River (Images taken from Gran et al., 2009; Gran et al., 2013).

Section 2: Background

2.1 Geologic Setting

The Greater Blue Earth River (GBER) basin is a subwatershed of the Minnesota River and is underlain by primarily Ordovician dolostones and glacial tills and outwash from extensive Pleistocene glaciation of the area (Jennings, 2010; Clayton and Moran, 1982). South-central Minnesota was glaciated by the Des Moines lobe of the Laurentide ice sheet (LIS) that advanced and retreated across the area numerous times. Following episodes of till deposition, water draining from the ice sheet continued to deposit glacial outwash (Clayton and Moran, 1982), now expressed as interbedded glaciofluvial sediments between till units. Following several periods of deposition of glacial till and outwash, glacial Lake Agassiz developed along the southern margin of the LIS. Water pooled in glacial Lake Agassiz drawing from approximately 500,000 km^2 of ice-covered land (Clayton and Moran, 1982; Teller et al., 1996; Thorleifson, 1996). Around 13,400 calendar years BP, near the end of the Wisconsinan glaciation, glacial Lake Agassiz first drained out the southern outlet, forming the Minnesota River Valley (Belmont et al., 2011b). This drainage resulted in the incision of the valley causing regional base-level fall and initiating the migration of knickpoints up the Blue Earth River, Watonwan River and Le Sueur River (Belmont et al., 2011a).

As the knickpoints in the GBER basin migrated upstream, they laid back, leading to the development of a knickzone instead of a discrete waterfall. Knickpoint migration leads to higher channel incision rates in the knickzone with lower incision rates upstream of the knickzone. This dichotomy results in two drastically different erosional

environments above and within the knickzone. Above the knickzone, the river has a relatively low gradient with very few ravines or bluffs. Below and within the knickzone, erosion of the bluffs delivers most sediment to the river (Gran et al., 2009; Belmont et al., 2011; Day et al., 2012).

It is assumed that network evolution of the Le Sueur River basin has expanded the drainage area since the time of base-level fall. Prior to the drop in base-level, the watershed was much smaller with internal drainage holding large volumes of water in lakes and wetlands, which comprised between 15% and 35% of the watershed (Marschner, 1930). Base-level fall resulted in incision that was translated through the system by ravine development. A model has been constructed to show long profile development through time using constant discharge (Gran et al., 2013). Results showed the Le Sueur River is best modeled as a detachment-limited system with downstream coarsening. The model used constant basin size, network structure, modern discharge, and hydraulic geometry relationships. However, the network has been expanding, which should lead to an increase in discharge over time. In addition, more recent changes in land use and climate should also lead to increases in discharge. Work has been done to show how recent changes in climate and land use affect discharge (Schottler et al., 2013). Here, we aim to extend that work back in time to quantify how large-scale changes to the watershed associated with drainage network evolution in addition to climate change and land use change affect discharge. What is the magnitude of channel change over the last 100 years versus the last 13,000? Which of these drivers dominates? Do we see a slow and steady increase in discharge through time due to network expansion, followed by a

slight increase at the end due to climate/land use changes? Or do we see relatively little change over the Holocene and then a large increase in the last 100 years? This research aims to address these questions by determining the pattern of change in channel geometry and discharge over the Holocene.

2.2 Climate and Discharge

There are records of climate excursions throughout the Holocene, including both periods of warming and cooling (Mayewski et al., 2004). The global paleoclimate record documents fluctuations in the global climate that have occurred regularly throughout Earth's history. The most dramatic climate fluctuations during the Holocene were the Little Ice Age (LIA) and the MHDP. The MHDP occurred from 4 to 9 ka and was much drier and warmer in Central Minnesota, as indicated by higher rates of loess accumulation in the Great Plains (Miao et al., 2005). The LIA occurred from 1650 to 1850 AD and was a time of cooling, approximately 1 degree drop globally (Winkler et al., 1986). Climate change over the Holocene has been quantified by observing the past changes in vegetative boundaries; for example, the movement of spruce-dominated forests north, in response to changes in climate, and then their return south (Bartlein et al., 1984).

Changes in climate have occurred over shorter timescales, too. Global temperatures from the past 15 years show a deviation from the average temperature from 1895 to 2014 (Figure 2.1) (IPCC, 2014). In Minnesota, studies of climate have shown that temperatures have increased over the past 100 years (MN CWG). Over the same timeframe, there has been an increase in discharge in many major rivers in the state of Minnesota, as well as increases in precipitation (Novotny and Stefan, 2007). Climate and

land use changes have resulted in increased streamflow (Novotny and Stefan, 2007), and there is a direct correlation between precipitation increases and discharge increases in the state of Minnesota (Schottler et al., 2013).

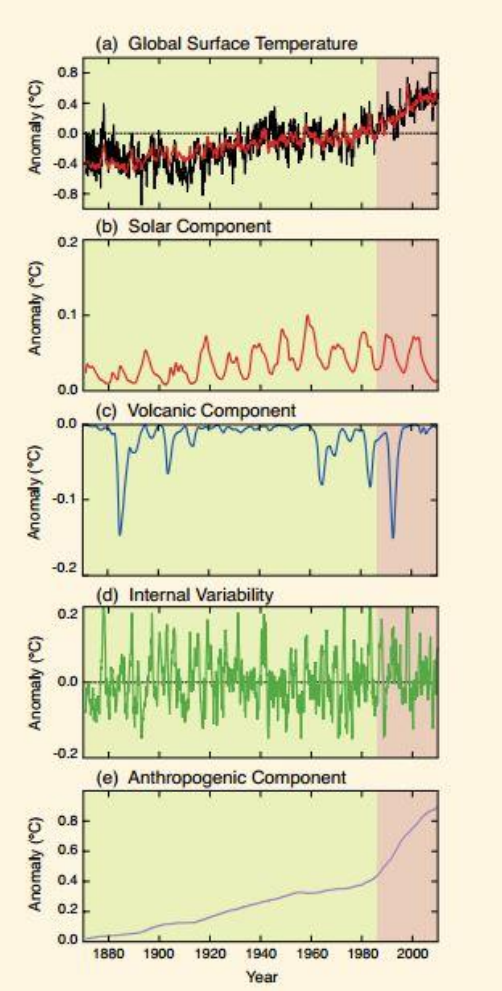

Figure 2.1. An image obtained from the Intergovernmental Panel on Climate Change (IPCC) 2014 report showing (a) changes in global surface temperature, (b) variations in solar activity, (c) changes in temperature due to volcanic activity, (d) internal variability in climate, and (e)the anthropogenic component of climate change over the period 1870 to present.

There is a direct relationship between changes in climate and the response of rivers to this perturbation. Climate and weather impact a river's geomorphic character as it sets a balance between erosion and deposition. Changes in the timing and magnitude of precipitation impact discharge (volume/time), which in turn controls the channel width, depth, gradient, sediment load, and much more.

2.3 Land Use

Land use is another factor that plays a major role in drainage network and channel development. Prior to European settlement, vegetation was abundant along the rivers; and much of south-central Minnesota was classified as prairie and wet prairie or marsh in the uplands, with hardwoods and river bottom forest in and along river valleys (MN DNR, 1988; Marschner, 1930). Currently, more than half of the state of Minnesota is farmland, with very little grassland. Within the GBER basin, farmland makes up 90+ % of land use. More importantly, there has been a drastic decrease from 15-35% to 5.7% of area of wetlands because they have been drained to make room for more crops (http://land.umn.edu/quickview_data/index.html) (Figure 2.2).

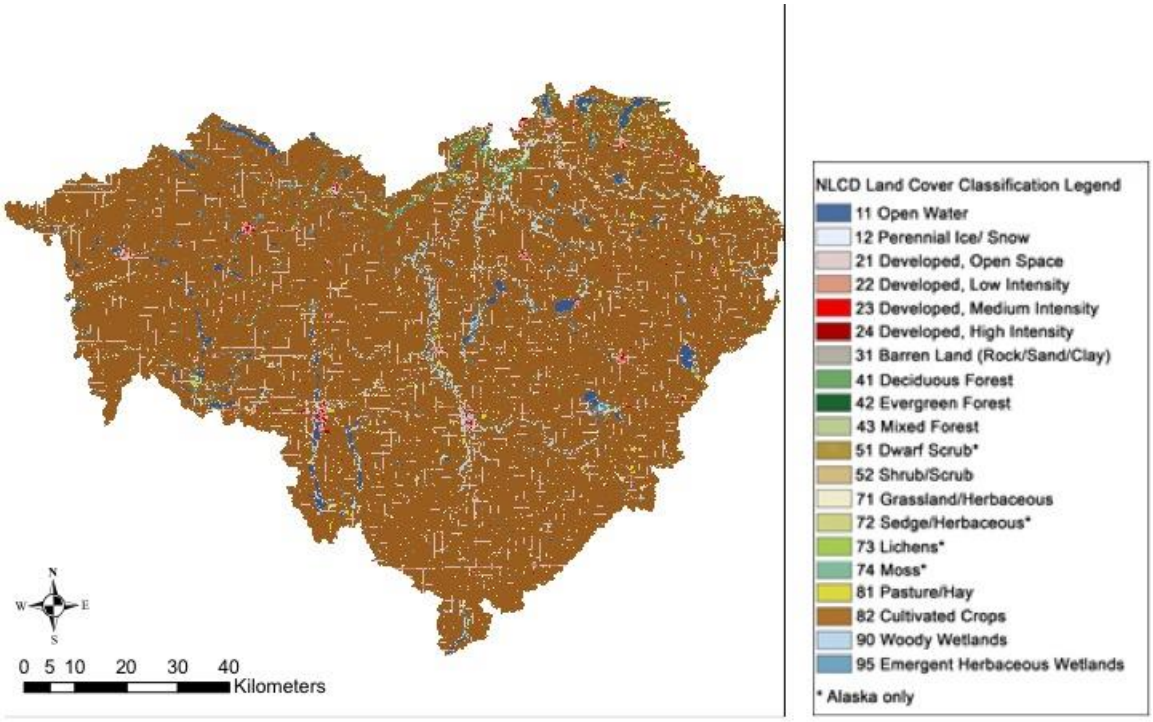

Figure 2.2**.** Land use in the Greater Blue Earth River (GBER) basin from the National Land Cover Database (NLCD) 2006.

Around 1820, European settlement began in Minnesota, particularly around rivers due to their ability to transport materials. Settlement continued to grow throughout the area; and, around 1860, farmers began growing wheat in Minnesota. Over the next 10 years (1860-1870), the population of Minnesota grew by 255% reaching almost 450,000 (Minnesota Historic Farms Study, 2006). By the late 1870's, wheat was being farmed on almost 70% of land.

In the 1890's, farming developed rapidly. As more people began to farm, there was a demand for land (Minnesota Historic Farms Study, 2006). This resulted in the mass draining of wetlands to open up new areas for more farmland. Ditches were dug to collect water and deliver it to rivers and lakes. Artificial subsurface drainage (tile drainage) was installed by landowners to expedite the process of field draining, thus extending the growing season. This practice is characterized by a drain composed of plastic tubing, concrete, or clay buried in the subsurface. The overlying ground is perforated, in order to aid in quick delivery of water to the drains (Tile drain installation and repair, IN.gov, 1996). In 1910, there was the "peak of public drainage ditch construction" led by the leader of the tile drainage effort, James J. Hill. Within a five year period, drainage was installed in over six million acres of land in Minnesota. One-third of the state's farmlands were installed with drainage by the 1960s (http://land.umn.edu/quickview_data/index.html). Tile drainage continues to be used by private landowners in agriculture. Drains are being installed in closer proximity and varying depths that increases the density of drains. As of 2000 AD, there were more than 600 miles of tiled drains in the Le Sueur River watershed alone (Water Resources Center,

2000a). Referring back to changes in streamflow, it has been determined that changes in climate and agricultural crop conversion are only accountable for approximately 50% of the increased streamflow, with the remainder of the increase attributed to artificial drainage (Schottler et al., 2013).

2.4 Sediment

Under section 303d of the federal Clean Water Act, the Minnesota River has been classified as impaired for turbidity due to high amounts of fine sediment (Belmont et al., 2011). Turbidity is a measure of the clarity of water, which factors in sediment and biotic inputs. The Minnesota Pollution Control Agency (MPCA) standard for non-trout streams for turbidity is 25 Nephelometric Turbidity Units (NTUs) (MRB TMDL Project for Turbidity, 2011).

Excess sediment loads entering rivers are controlled by a balance among geology, climate, and land use. Since the underlying geology of the MRB has not changed within the time frame of changes in sediment load, changes in climate and land use are the 2 main factors contributing to changes in sediment load over the past two centuries. A previous study within the Le Sueur River completed an analysis to quantify changes in discharge due to climate and land use change (Schottler et al., 2013). The Le Sueur River shows significant changes in water yield (flow over watershed area) and runoff ratio (water yield divided by precipitation) between two 35-year time periods (1940-1974 and 1975-2009) (Schottler et al., 2013). This change was attributed to both climate and artificial drainage.

An increase in discharge has a direct impact on sediment loads in rivers by widening channels through erosion of bluffs and banks. Erosion and incision add more sediment to the river, where it may end up in the Minnesota River floodplain, GBER floodplain, Le Sueur River floodplain, the Mississippi River, or Lake Pepin (Gran et al., 2011; Schottler et al., 2013; Belmont et al., 2011a). Looking specifically at the Le Sueur River, based on aerial photos, the channel width has increased from 13 meters to 38 meters from 1949 to present, which corresponds with an increase in discharge obtained from the Red Jacket stream gage.

Sediment cores taken from Lake Pepin show that since the introduction of agriculture, sediment delivery to Lake Pepin has increased 10-fold, determined from Lake Pepin sediment cores (Engstrom et al., 2009). Prior to European settlement, most of the sediment was derived from near-channel sources. This changed in the early 1800's, with a shift towards sediment derived from agricultural fields, which make up about 90% of the watershed (Belmont et al., 2011; Gran et al., 2009). With the introduction of soil conservation practices, farmers have decreased the amount of sediment coming from the uplands; however, the net sediment export did not change. Now, sediment entering the major tributaries of the Minnesota River is mainly from near-channel sources (Belmont et al., 2011). Currently, approximately 1% of the landscape is responsible for approximately 70% of the sediment entering the Upper Mississippi River at the confluence with the Minnesota River (Belmont et al., 2011). As flows increase, these sources of sediment are increasing, too. Because of modern sediment issues and the record at Lake Pepin, people are interested in understanding what the sediment flux was through time. Erosion rates

were approximately 4 times lower in the valley in pre-settlement times compared to current conditions (Gran et al., 2013), as determined through numerical modeling, however that modeling was done assuming a static watershed and no change in discharge. We want to place better constraints on paleodischarge as another approach to understanding pre-settlement sediment flux.

2.5 Terraces and Paleochannels

Paleochannels are preserved throughout the GBER basin on terraces. A terrace is an abandoned floodplain that sits higher in elevation than the active floodplain; abandonment depends on changes in climatic or tectonic conditions, or a combination of both. Meander cutoffs preserved on terraces can represent a snapshot of a river's form at an earlier time.

Terraces form as the river erodes laterally and are stranded and preserved when incision cuts them off from the current river. Strath terraces are erosional terraces carved into bedrock and capped by alluvium. Terraces are confined within the river valley and resemble steps approaching the valley floor and increase in age with increase in elevation from valley floor. Terraces can be paired or unpaired (Figure 2.3). Paired terraces have terraces of equal elevation on both sides of the river; whereas, unpaired terraces are staggered in elevation across a river valley, taking the appearance of steps. Both types represent passing of time in the river’s history (Ritter et al., 2006). Preservation of these features allows for reconstruction of river history.

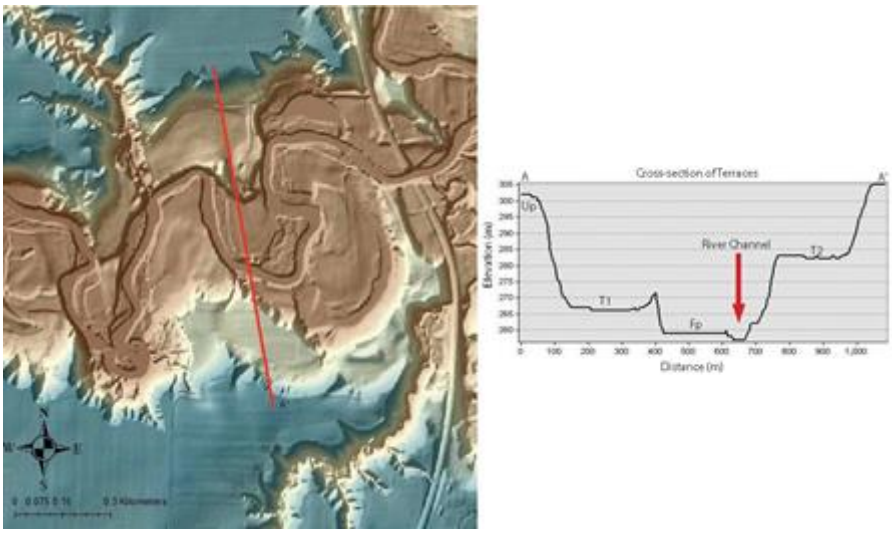

Figure 2.3**.** Aerial view of terraces located on the Le Sueur River, a tributary to the Minnesota River. The cross-section from A to A' shows the elevations of the terraces and their relation to the river channel. These terraces are unpaired.

Terrace preservation is due to a balance between lateral planation (lateral erosion) and vertical incision (downcutting). Lateral planation, which carves the terraces, occurs over a relatively long time scale. Vertical incision, which strands the terraces, occurs over a relatively short time scale (Wegmann and Pazzaglia, 2002). Changes in erosional regimes depend on changes in environmental factors.

The chronology of environmental changes can be determined by dating terraces; however, a lag time needs to be accounted for. This is the time delay between the change in conditions and the river's response. For example, straths may form during glacial cycles where high sediment loads allow for lateral planation and are preserved when low sediment loads result in vertical incision (Hancock and Anderson, 2002). After the sediment flux changes, it takes time for the river to respond.

Terraces have been forming in the MRB due to base-level fall of approximately 70 meters, which occurred around 13.4 ka (Belmont et al., 2011). As the rivers eroded both laterally and vertically, unpaired terraces formed at descending heights and ages which allow construction of a detailed history of their development and the river's response to base level fall (Gran et al., 2013). These terraces are strath terraces, cut into the dense glacial till that underlies the GBER basin (Gran et al., 2013). On top of these terraces, fluvial features may be preserved in the alluvial cap.

Within the GBER basin, meander cut-offs can be identified from airborne lidar on terrace surfaces where the surface expression has been preserved. A meander cut-off is a meander bend that has been cut off from the river through avulsion, leaving behind an oxbow lake that is later filled in with overbank sediment. Within this meander cut-off,

characteristics may be preserved in the sediments and subsurface stratigraphy that allow for paleogeometry and thus paleodischarge estimations. However, obtaining paleogeometry is a complicated task. In the Mississippi River Valley, paleogeometry was obtained by Knox (2000) through coring closely-spaced areas and noting the change from channel fill to channel margin sediments, identifiable by a change from fine to coarse sediment. Here we image the subsurface through a combination of coring and ground penetrating radar.

2.6 Ground Penetrating Radar (GPR)

Underlying stratigraphy preserved on terraces can be characterized using the geophysical technique known as ground penetrating radar (GPR). Since its introduction, GPR has gained popularity in the geosciences because it allows data collection in the shallow subsurface to be quick and non-intrusive.

The balance between Maxwell's equations and constitutive relationships is the governing theory behind GPR. Maxwell's equations describe how the electromagnetic fields (Equations 1.1-1.4) behave and the constitutive relationships (Equations 1.5-1.7) are dependent on the material properties (Jol, 2009). These sets of equations are the basis behind how GPR operates. Electromagnetic signals are sent into a material and the resulting waves reveal changes in density, texture, grain size, composition, etc. of the material.

$$\nabla * E = -\frac{\partial B}{\partial t} \qquad 2.1$$

$$\nabla * H = J + \frac{\partial D}{\partial t} \quad (2.2)$$

$$\nabla * D = q \quad (2.3)$$

$$\nabla * B = 0 \quad (2.4)$$

Here, E is the electric field strength vector (V/m), q is the electric charge density (Coulomb/m^3), B is magnetic flux density vector (Tesla), J is electric current density vector (Amperes/m^2), D is electric displacement vector (C/m^2), t is time (s), H is magnetic field intensity (A/m). J, D, and B are related to E and H through the following relationships.

$$J = \sigma E \quad (2.5)$$

$$D = \varepsilon E \quad (2.6)$$

$$B = \mu H \quad (2.7)$$

where σ is electric conductivity (affects how quickly electromagnetic waves are attenuated), ε is dielectric permittivity (affected by moisture content), and μ is magnetic permeability.

GPR works by monitoring the two-way travel time of electromagnetic waves sent into a material., which is affected by the material's properties (Figure 2.4). The strength of the returned signal is linked to the change in dielectric permittivity at the interface. Smaller changes are represented by lighter reflections, whereas larger changes have strong, bold reflections. A complete image of the subsurface is possible through a series of energy pulses called a scan. The signal sent back shows a black/white contrasted image with reflections marking changes in electrical conduction or dielectric permittivity (geophysical.com). Stronger reflections represent more drastic changes from one material to the next. A signal moving from low permittivity material to high permittivity will result in a strong reflection. Some energy is reflected back to the unit to depict the subsurface, while the rest of the energy travels as deep as possible until the energy completely dissipates.

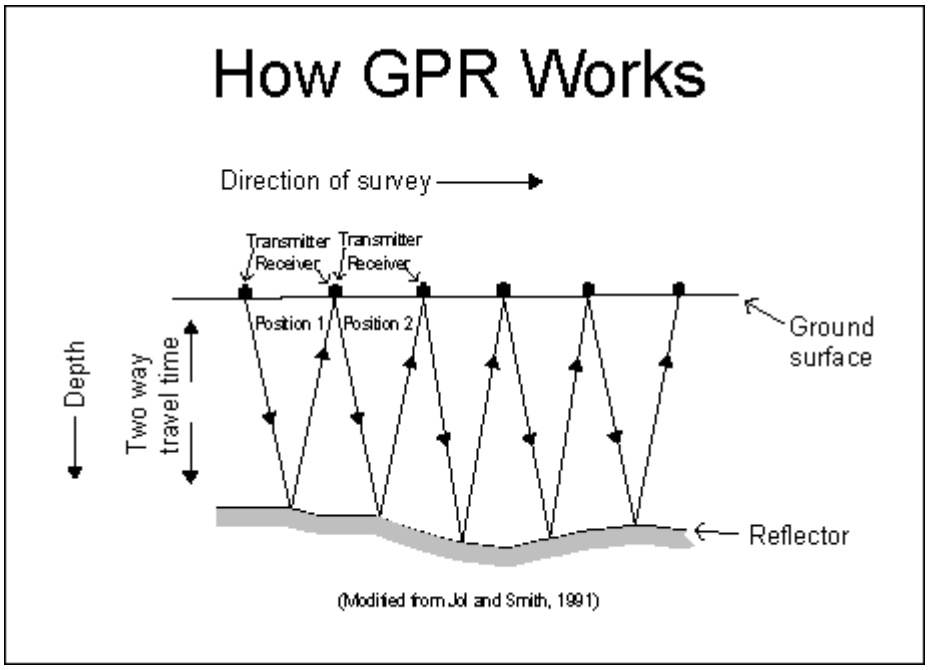

Figure 2.4. Schematic diagram of how GPR collects data of the subsurface using electromagnetic waves.

GPR units consist of a set of antennae that sits directly on the ground surface with a transmitter and receiver as well as an acquisition system that collects the receiver information. These two pieces of equipment are connected to one another through a series of fiber optic cables. The transmitter sends a signal into the ground at each location (specified by antenna frequency) and the reflected signal is detected by the receiver. It is then sent to the acquisition system that displays the data on the computer. Data are collected in real-time and are instantly available to describe and interpret subsurface stratigraphy even before data collection is complete (Jol, 2009).

Varying densities and composition of underlying sediment are identifiable in the data output, due to changes in wave characteristics. GPR velocity is determined by the dielectric permittivity, which is strongly influenced by soil moisture. The GPR can pick up these minute differences within sediment. There are numerous options for frequency of the antennae. Frequency used is based on the underlying geology. Lower frequency antennae (longer wavelength) will increase penetration depth, but decrease detail, whereas, high frequency antennae (shorter wavelength) will not penetrate as deep but can highlight finer variations within the material., such as stratigraphy. The data received give insight into the subsurface geologic materials.

Clays tend to attenuate the signal., preventing detailed images of the underlying stratigraphy. More specifically, a GPR wave of a fixed frequency, traveling through a subsurface composed of sand would travel deeper and have more detail than the same signal in a subsurface composed of clays, due to the higher conductivity of the clay-rich sediments. Sands typically have low conductivity allowing GPR signals to travel through

them with ease, whereas, clays are highly conductive, which causes a GPR signal to rapidly attenuate. Although detailed images of bedding and structures within clay are hard to obtain, due to the high contrast of dielectric permittivity at the boundary, the interface between clay and another medium is easier to identify (Bristow and Jol, 2003).

2.7 Optically Stimulated Luminescence (OSL) dating

Optically Stimulated Luminescence (OSL) dating is a technique used to determine the burial age of quartz sediment up to 150 ka years ago (Ankjaergaard, 2012). Radiation from the decay of potassium, thorium, and uranium present in sediments affects in-situ quartz grains. A single grain of quartz absorbs radiation from the decay of U, K, and Th. Over time it accumulates within an individual quartz grain at a particular rate. Radiation is stored within ‘traps’, in the grain, which cause electrons to jump from one energy level to the next. The rate at which energy gets "trapped" is unique to a particular grain and is called the dose rate. When electrons become excited, they become trapped in the new location. This energy stored by the electrons can be released through either heat or light stimulation, which returns the trapped charge to its original state (Madsen and Murray, 2009). In OSL, light exposure empties the radiation trapped within the grains. In the process of the electron returning to its original location, energy, in the form of protons, is released and can be measured. This energy is directly proportional to the amount of time the sediment has been removed from light or heat.

Bleaching is the process of light emptying the traps and resetting the particular grain to zero. Essentially, it resets the clock. Partial bleaching occurs when a grain's traps have not been completely reset (emptied), which can occur when grains are exposed to

some light, as in turbid water, but is not enough to fully empty the traps. This can also happen through a short exposure time. Partial bleaching is problematic for OSL dating, especially in fluvial sediments. This could result in an inaccurate age older than the feature being dated. The best way to increase confidence in OSL dates is to collect several samples within a given location. The Single Aliquot Regeneration (SAR) method is the best approach to obtain an accurate burial age for fluvial sediment (Wallinga, 2002). The SAR method dates individual quartz grains within a sample and averages the age for the entire sample. In order to estimate an accurate age, at least 30 aliquots need to be run. If partial bleaching has occurred, then a minimum age model can be used to obtain the most accurate burial age.

Section 3: Methods

To study changes in discharge through the Holocene in the MRB, I chose to work in one of the major tributaries to the Minnesota River, the Le Sueur River. The Le Sueur is located in south-central Minnesota in the GBER basin; the Le Sueur River enters the Blue Earth River 5 km from the Minnesota River. Paleomeanders were identified on terraces using 3 meter digital elevation model (DEM) data, with cross-sectional data obtained from GPR transects and sediment cores across paleochannels whose topographic expression was preserved on the surface. Paleogeometry was used to calculate discharge through a variety of techniques, and paleodischarge estimates were coupled with depositional ages on terraces to develop the discharge history of the river. Here I discuss my criteria for site selection, how GPR data were collected and processed to determine cross-section geometry, two methods of determining velocity for discharge calculations, and how paleodischarge estimates were compared to modern and historic bankfull discharges. This section concludes with a discussion of depositional age determinations via OSL, and a valley evolution model used to determine depositional ages for study sites.

3.1 Site Identification

A 3 meter lidar-derived DEM of the GBER basin was used to identify meander bend cutoffs preserved on terraces. These features are paleochannels, relicts of old river channels. In order to collect data that represents spatial and temporal variation, I selected paleochannels at varying heights above the modern channel and distances upstream from the confluence with the MN River (Table 3.1). Both are a proxy for age; older terraces

are found at higher elevations and further downstream. Once I selected 5 paleochannels, I used *Beacon Property Information* website, which is unique to Blue Earth County, to contact landowners to work on their property. Once sites and property owners were identified, I contacted landowners via phone to obtain permission.

Table 3.1. List of paleochannels and respective locations.

Site ID	Height above channel (m)	Distance upstream from MN River (m)	UTM coordinates
LS01	23	8270	15 N 0416749/4885138
LS02*	5	8270	15 N 0416770/4884669
LS03	6	9970	15 N 0416790/4883714
LS05	7	21270	15 N 0421051/4882226
LS06	4	21470	15 N 0421206/4882169

* Le Sueur Site 2 (LS02) was excluded from calculations due to poor quality of GPR data.

3.2 Estimating Geometry

GPR profiles were collected to obtain data on subsurface stratigraphy in order to determine paleochannel cross-sectional geometry as preserved on terrace surfaces. I placed the 3 GPR lines within each paleochannel, perpendicular to the flow of the paleochannel and used a 100 MHz antennae and DVL III supplied by Sensors and Software Co. The antennae were connected to the computer and the console through a series of fiber optic cables and powered by a car battery. Parameters used for all sites were based on underlying geology, depth of penetration needed, and antennae frequency

(Table 3.2). An elevation profile along the transect was surveyed using an autolevel and stadia rod to place topographic data on the GPR lines to estimate accurate depths to reflectors.

Table 3.2. Parameters set in DVL III computer system for GPR data collection.

Parameter	**Setting**
Paddle separation distance	1 meter
Step size	0.25 m
Start location	0 m
Antenna frequency	100 MHz

All of the GPR lines were processed using the same parameters (Jol, Morrison personal communication; Table 3.3). All data processing for GPR was done using the Sensors and Software program Ekko Project 2. The lines were displayed using the wiggle trace with shading to the right to highlight important reflectors. GPR data are measured in time rather than depth. In order to convert from time to depth, wave velocity in the sediment is multiplied by time. Once the GPR data were processed and the topography applied, lines were described. I described the shape, continuity, dip angle, and thickness of prominent reflections. I use the word ‘packages’ to describe sets of dipping reflections that appeared to coincide with one another.

Table 3.3. Steps for processing GPR data in Ekko Project 2.

Processing tools	**Defined**
Automatic gain control (AGC)	Sharpens image and boosts weaker reflections
Dewow	Removes excess low frequency noise from the data
Horizontal filter	Averages horizontal traces together for higher quality image.
Vertical filter	Averages vertical traces together for higher quality image.

To aid in the interpretation of GPR data, sediment samples were collected along each line. Sediment cores were obtained two ways; 1) hand augering and 2) a Giddings Core machine supplied by the Minnesota Geological Survey (MGS). These were used to validate the GPR profiles. Samples taken at various depths can help interpret the GPR data by defining the reflections. I selected approximately 5 locations along each line to core to identify the paleochannel boundaries. Samples were sieved using an automatic sieve with fractions ranging from No. 4 to No. 200 or 4.76 mm to 0.074 mm, respectively. Data were compiled for each GPR line and placed on the line in their corresponding locations.

Changes in grain size obtained from sediment samples were placed on GPR lines to highlight important reflectors, simplifying boundaries of each paleochannel. Most importantly, the cores show depth to refusal., which was assumed to represent the base of

the paleochannel. I assumed the shape of the paleochannel obtained from cross-sectional view is representative of the bankfull discharge, equivalent to the 1.5- to 2-year flood in an equilibrium channel. Paleogeometry is the first step in calculating the discharge of an abandoned river channel. Using the GPR profiles and sediment samples, I identified the best estimation of the boundaries of buried paleochannels to determine paleogeometry including wetted perimeter, cross-sectional area, width, depth, and hydraulic radius. Paleoslope was assumed to be the same as the modern slope, which was obtained from field data (Belmont, pers. comm.). These estimations must include associated errors. I determined error in 2 ways: 1) instrumental error was accounted for by applying a +/- 0.5 meters to width and depth measurements (Jol and Bristow, 2003) and 2) alternative channel boundaries were identified where relevant, resulting in a range of discharges for some sites.

I also estimated paleogeometry using 3-m resolution airborne lidar (light detection and radar) data. Paleochannels were initially identified by their surface expression, so I measured the geometry associated with the surface expression to see if it could represent the channel form. I used the lidar data to obtain the cross-sectional width of the channel and used width-to-depth ratio relationships, from the modern channel, in order to estimate depth, assuming that, over time, a river will maintain approximately the same width-to-depth ratio.

3.3 Velocity

The next step to calculate paleodischarge is to estimate velocity of water in channel at bankfull stage. Velocity was estimated 2 ways: (1) Manning's Equation and (2) Law of the Wall.

3.3.1 Manning's Equation

Manning's Equation estimates the velocity of a river by relating velocity of water to cross-section channel geometry, water surface slope, and bed roughness:

$$u = \frac{1}{n} R^{2/3} S^{1/2} \qquad 3.1$$

where u is velocity (m/s), k is 1 for SI and 1.49 for English units, n is Manning's roughness, R is hydraulic radius (m), and S is slope. In order to apply Manning's Equation, I assumed bed roughness and channel slope were the same as current values; I estimated bed roughness from a table of values defined by channel characteristics (Chow, 1959) and local channel slope from field measurements (Belmont pers. comm.). Paleodischarge is the product of cross-sectional area and velocity. Due to a wide range of variability within the Le Sueur River, I also completed a sensitivity analysis with a range of Manning's n values +/- 0.01 on either side.

3.3.2 Law of the Wall

The Law of the Wall describes a turbulent velocity profile and can be used to calculate velocity at a particular location in the water column. Velocity is estimated using

$$u = \left(\frac{u^*}{k}\right) ln\left(\frac{z}{z_0}\right) \qquad 3.2$$

where u_* is the shear velocity, κ is the von Karman constant, z is the height above the bed at the point of interest, and z_0 is the measure of roughness. Before applying this equation, several variables need to be determined. Shear stress (τ) was calculated using the reach-averaged equation:

$$\tau = \rho g h S \quad (3.3)$$

where ρ is the density of water, g is the gravitational force, h is the depth at the thalweg and S is the local slope; using the thalweg depth results in an estimation of maximum velocity. Shear velocity (u*) can be calculated with the equation,

$$u^* = \sqrt{\tau/\rho} \quad (3.4)$$

The bed roughness, z_0, is calculated using the equation

$$z_0 = D_{50}/30 \quad (3.5)$$

Where the D_{50} is median grain size (m). Grain roughness was estimated by taking the measured D_{50} from the field (20 mm) highlighting the coarsest D_{50} located closest to the confluence with the Minnesota River (Gran et al., 2013). The Law of the Wall equation

was used to determine mean velocity, which was multiplied by the cross-sectional area to determine paleodischarge.

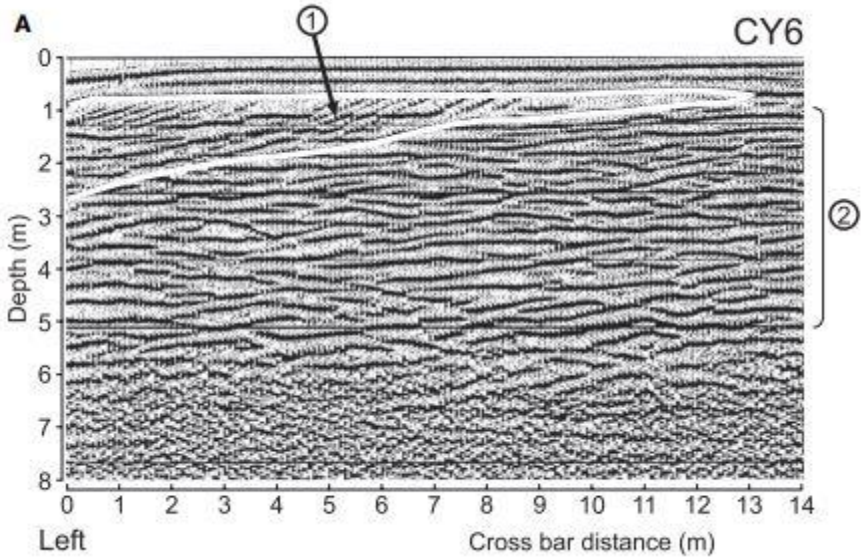

Figure 3.1. Example of GPR line showing signature of a sandy river in the subsurface. 1 represents lateral migration and 2 represents the alluvial package. Line was taken from Sambrook Smith et al., 2006.

3.4 Historic and Modern Discharge

As a way to confirm paleodischarge calculations, I completed the same calculations on the current channel using geometry collected from field measurements (Belmont, pers. communication). I also used historic aerial photos to estimate changes in channel geometry over the past 75 years. I measured channel widths from 1940, 1950, 1964, 1991, and 2003 at several locations within the knickzone, which is located within the lower 40 kilometers, referenced from the confluence with the Blue Earth River. More specifically, all measurements were made within the lowermost 5 km of the Le Sueur River, referenced from the confluence with the Blue Earth River. I used Equation 3.6 to estimate depth in the historic channels, based on width-to-depth relationships obtained from field measurements in the modern channel.

$$h = \frac{b:h}{b} \qquad 3.6$$

Where *b* is width (m), *h* is depth (m), and *b:h* is the width-to-depth ratio of the modern channel. Once depth was determined, I used historic data (obtained from USGS stream gage #05230500) to assign a discharge value for the date the aerial photo was taken. It is not likely the aerial photos were representative of bankfull, but are representative of a particular time period. Since this is used to show changes over time, I have determined that comparing the highest discharge of older channels and the lowest discharge of current channels, should still show variation in widths and therefore, discharge.

3.5 Flood Frequency Analysis

To determine discharge for the 1.5 and 2-year flood events, I ran a Log Pearson III analysis on peak streamflow data for the past 70 years from the Le Sueur River USGS stream gage at Red Jacket (#05230500) (http://streamflow.engr.oregonstate.edu/ analysis/floodfreq/). Flood frequency analyses were used to determine which size event most clearly matches the bankfull discharge as estimated from channel geometry, with the prediction that it would be in the 1.5 to 2-year flood range. I compared the estimated bankfull discharge from the log Pearson III analysis and from current channel geometry using the same steps explained above to test the techniques used to determine bankfull discharge from field data.

I completed the same Log Pearson III analysis using 30-year increments from the entire dataset. Increments included: 1930-1960, 1940-1970, 1950-1980, 1960-1990, 1970-2000, and 1980-2013. I compared the modern discharge with historic discharge data and paleodischarge data from terraces to assess how discharge has changed through time.

3.6 Chronology

Optically stimulated luminescence (OSL) samples were collected following the Utah State University (USU) Luminescence Laboratory sampling procedures (http://www.usu.edu/geo/luminlab/). Samples were collected at greater than 1 meter depth using a light-proof tube (aluminum). A dose rate sample was collected in a Ziploc bag, and water content samples were placed in waterproof containers. All of these factors

influence the processing and age calculations. Dating was completed at USU, in Logan, Utah, under the instruction of Dr. Tammy Rittenour and her lab technicians. Eighteen samples were processed through to the hydrofluoric acid stage. A brief description of the processing is described below and a more detailed explanation of sampling and processing can be found in Appendix I. Before starting any processing, all samples were logged in to the USU lab with a USU number (Table 3.4). Additional samples collected and processed for the Blue Earth River are listed in Appendix III.

Table 3.4. List of all sites where an OSL sample was collected for this project including UTM coordinates, height above channel, and distance upstream.

Site ID	Easting	Northing	Height above Channel (m)	Distance Upstream (m)
LS01	416749	4885138	23	8270
LS02*	416770	4884669	5	8270
LS03	416790	4883714	6	9970
LS05	421051	4882226	7	21270
LS06	421206	4882169	4	21470

Water content was determined first by weighing an empty beaker on the scale and recording the weight. The air-tight container was emptied into a beaker (labeled with the USU #- H_2O) and its new weight recorded. The beaker was placed in the oven (approximately 40 degrees C) to sit overnight. Dry samples were removed from the oven and placed in the desiccator for no longer than 30 minutes for sediment to reach room temperature. The sample was reweighed and the final weight recorded in the dose rate book. Water content was calculated using 3.7.

$$\%H_2O = \left({}^{original\ wt}/_{final\ wt} \right) * 100 \qquad 3.7$$

Dose rate was not completed at the USU lab; samples are sent out to another lab and then used to determine the age. Preparation for dose rate in the USU lab includes collecting a 25-50 mL representative sample of the sediment. The actual sample that will be exposed to light then goes through a process of steps completed in a dark room to get it ready including sample extraction, wet sieve, HCl treatment, bleach treatment, float, and HF treatment. All of the samples that I processed in the lab were treated with bleach and dried.

Due to the small number of OSL labs in the nation and the large number of samples run at each particular lab, preliminary OSL ages take anywhere from 6 to 9 months and the actual ages take 1-2 years. Therefore, I also used a 1D Le Sueur River incision model (Gran et al., 2013) to compare with the OSL ages of the paleochannel terraces in the Le Sueur River.

Results

4.1 GPR line descriptions

In order to estimate paleogeometry, the processed GPR lines were described in detail to increase our understanding of the subsurface through reflection relationships. Given the poor quality of the GPR data and the lack of sediment cores, Le Sueur Site 2 and Le Sueur Site 1C were removed from further data analysis. The geometry of the surveyed paleochannels was determined from the measured GPR lines and airborne lidar. Three results are presented: 'best interpretation' from GPR (presented as range), uncertainty estimates from GPR, and surface expression from lidar.

Using data obtained from sediment samples and depths, I estimated the best possible geometry for each paleochannel based on processed GPR data. The description and interpretation from one site (LS3A) is below, with all other descriptions and interpretations in Appendix 2, excluding LS01C and LS02 due to poor data quality.

> *Le Sueur Site 3A Description: At start of the line (0 m), there are clear 'air waves' in the deeper subsurface throughout the first 10 m. Within the first few meters (~2), there are semi-continuous, gently-dipping reflections for about 50 m. Then reflections flatten for about 15 m where they begin to gently dip upwards. The package of dipping reflections becomes larger at 70 m. At 80 m, the dipping reflections flatten out and become sub-horizontal; the reflections penetrate deeper at this point and continue to the end. Within this complex package, there are semi-continuous, hummocky reflections, overlain by sub-horizontal reflections. Gently-dipping reflections go in either direction (Fig. 4.1).*

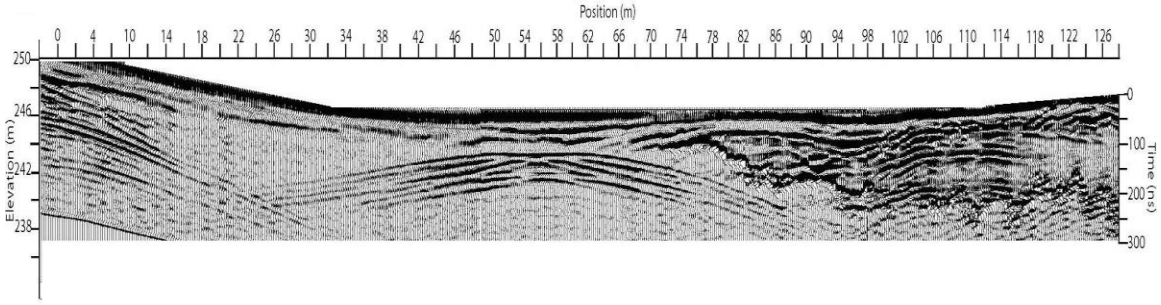

Figure 4.1. Image of processed GPR line at Le Sueur Site 3A.

4.2 Paleogeometry

The ‘best interpretation’ of paleogeometry was obtained from combining the interpreted GPR data and the sediment core data to identify channel boundaries. From the processed GPR line (Figure 4.1), channel forms can be identified. Placing the core data on the lines further validates the channel geometry; assuming coarser sediment, especially large gravels, represents the base of the channel (figure 4.2). Then, the channel shape is placed on the line to determine the ‘best interpretation’ geometry (Figure 4.3; Figure 4.4). Due to the subjective manner at which the channels were selected, I highlighted potential variations in channel dimensions only when applicable (Figure 4.5). Therefore, the 'best interpretation' is presented as a range, in certain cases. The channel should maintain the same width-to-depth (*b:h*) ratio through time, allowing us to check estimated geometries within this range. Current channel width-to-depth ratios range from 15-20 based on field data (Belmont, pers. communication, 2015). Using the estimated paleogeometry, I calculated the *b:h* ratios for each line. Most sites fell within the range, however Le Sueur Site 1 and Le Sueur Site 6B have larger ratios (Table 4.1).

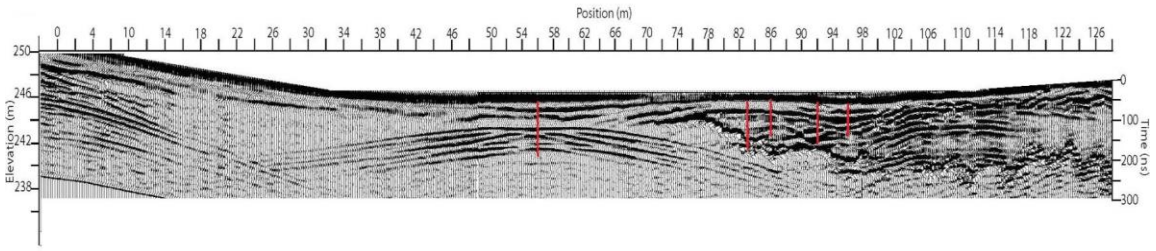

Figure 4.2. Vertical lines represent core data collected at Le Sueur Site 3A. These data were used to aid in identification of paleochannel boundaries.

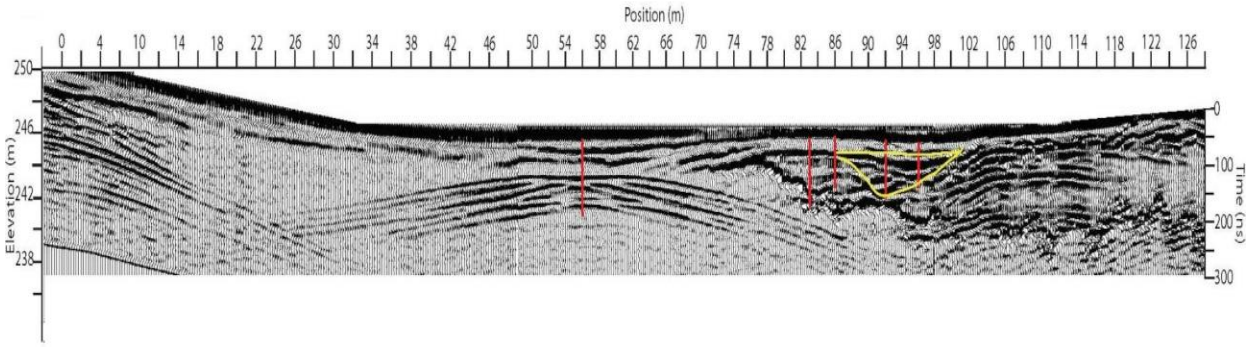

Figure 4.3. Image showing identified paleochannel boundaries, or ‘best interpretation’ channel for Le Sueur Site 3A.

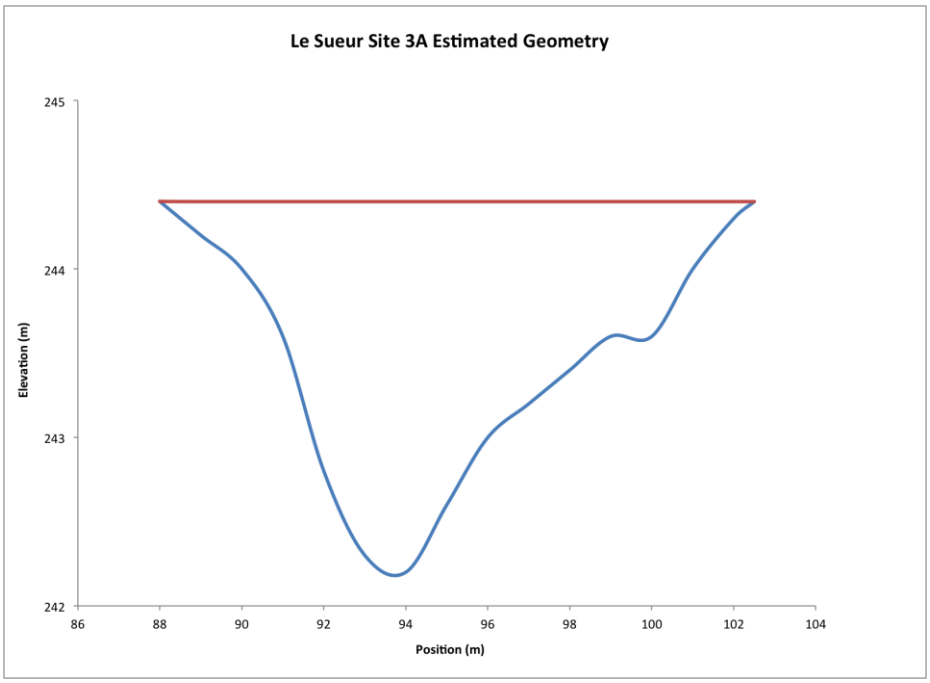

Figure 4.4. Cross-sectional view of paleochannel take from GPR line at Le Sueur Site 3A.

Table 4.1. Site locations and their estimated widths and depths from GPR lines; and the calculated width-to-depth ratio.

Site	Width (m)	Avg. Depth (m)	b:h Ratio
1A	30	0.9	34
1B	34	1.3	27
3A	15	1.0	15
3B	16	1.0	15
3C	17	1.1	16
5A	30	1.7	17
5B	14	0.8	18
5C	17	0.9	19
6A	15	0.9	17
6B	19	0.9	21
6C	19	1.2	15

There are two sources of error associated with the 'best interpretation' estimated paleogeometry: 1) instrumental error and 2) identification of the channel boundaries. Instrumental error was accounted for by adding an error of +/- 0.5 m to each channel based on Jol and Bristow (2003) criteria. The highest value for 100 MHz in saturated sand was 0.3, which was increased to 0.5 to account for silt/clay content. The channel boundary error was included by identifying a maximum and/or minimum channel where applicable. Some paleochannels have, in my opinion, a clear channel distinction that needed no alternative. Le Sueur Site 3A is presented below as a case study (Figure 4.5).

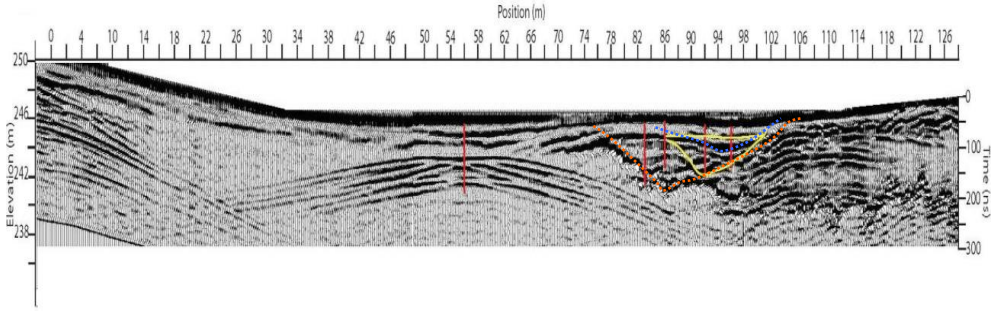

Figure 4.5. GPR image of Le Sueur Site 3A showing potential variations in channel boundaries. Dashed lines represent minimum and maximum while the solid line represents the ‘best interpretation.’.

Alternatively, there is a surface expression visible from airborne lidar that shows a channel form, which was also analyzed to determine if this shape could be the preserved paleochannel. Surface expression geometries were obtained through airborne lidar (Figure 4.6). Widths were obtained from the channel form as expressed on the surface from 1m airborne lidar. Using width-to-depth ratios, I estimated the depth needed to keep widths consistent with ratios. Estimated depths range from 4 to 18 meters (Table 4.2). This value is large, so when calculating the cross-sectional area for surface expression paleodischarge, I used the maximum depth to till from the GPR profiles. The average current bankfull depth of the Le Sueur River is 3.3 meters (Belmont pers. communication), and the river has incised and widened over the past century (Belmont et al., 2011). Therefore, the geometry estimated from lidar surface expression is likely too high and indicative of another form, possibly the floodplain. More specifically, the channel expressed on the surface is the integrated channel, which has migrated over the floodplain.

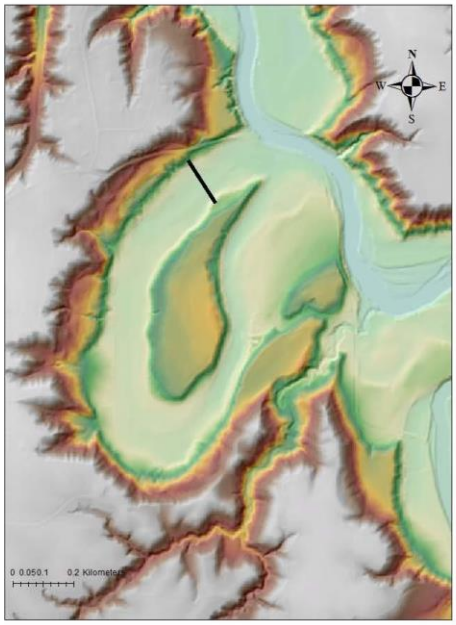

Figure 4.6. Image taken by airborne lidar of Le Sueur Site 3A showing surface expression.

A previous study measured the floodplain widths of the current Le Sueur River and found that floodplain width, within the knick zone, ranges from 75-225 meters, averaging around 125 meters (Belmont, 2011b). Field measurements of the paleochannel widths were combined with lidar-based paleochannel widths to compare the relationship. Assuming the surface expression is not representative of the paleochannel, but rather the floodplain, I compared modern channel-to-floodplain ratios with the GPR-based paleochannel width and the surface expression paleochannel width from lidar.

GPR-based paleochannel width to surface expression width ratios range from 0.06 to 0.36 and modern channel-to-floodplain width ratios are approximately 0.29 (Table 4.3). Smaller ratios represent narrower channels and/or wider floodplains, whereas,

higher ratios represent wider channels and narrower floodplains. Although the range is large, most of the estimated ratios are similar to the modern river. Most ratios are smaller, which means the channel is either smaller or the floodplain is larger compared to modern conditions. This suggests that paleogeometry estimated from surface expression is not representative of past river channel conditions, but rather represents the paleofloodplain.

Table 4.2. Table showing estimated widths from surface expressions and the calculated depths.

Site ID	Channel form width from lidar (m)	b:h ratio	Depth from b:h ratio (m)
LS01A	135	15	9
LS01B	95	15	6
LS01C	92	15	6
LS02A	188	15	13
LS02B	174	15	12
LS02C	182	15	12
LS03A	177	15	12
LS03B	235	15	16
LS03C	264	15	18
LS05A	118	15	8
LS05B	85	15	6
LS05C	88	15	6
LS06A	65	15	4
LS06B	71	15	5
LS06C	75	15	5

Table 4.3. Channel comparing width of channel to surface expression width and ratios of modern channel to floodplain widths.

Site	Channel width from GPR (m)	Surface expression width from lidar (m)	Channel width:surface expression ratio	Current Channel:current floodplain ratio
1A	30	135	0.22	0.29
1B	34	95	0.36	0.29
3A	15	177	0.08	0.29
3B	16	235	0.07	0.29
3C	17	264	0.06	0.29
5A	30	118	0.25	0.29
5B	14	85	0.16	0.29
5C	17	88	0.19	0.29
6A	15	65	0.24	0.29
6B	19	71	0.27	0.29
6C	19	75	0.25	0.29

The modern channel of the Le Sueur River in the lower 68 km, as measured in 2008 and 2015, has an average width of 33 meters and 39 meters, respectively; and an average depth of 2 meters and 2.58 meters, respectively (Belmont pers. communication). Figure 4.7 shows a cross-section of the Le Sueur River located 1.94 kilometers upstream of the confluence with the Blue Earth River. The channel dimensions for paleochannels and the modern channel were used to estimate paleodischarge and current discharge, respectively.

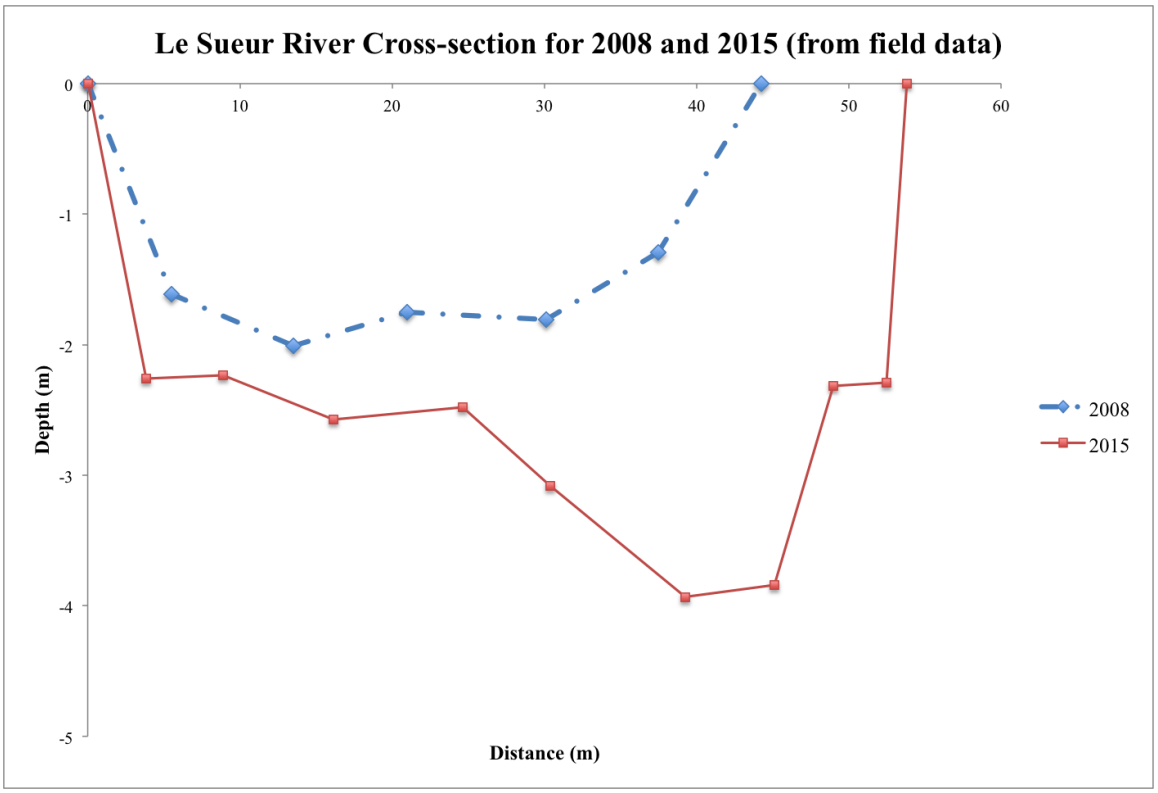

Figure 4.7. The solid line represents 2015 cross-section and the dashed line represents 2008 cross-section, both collected from field data.

4.3 Paleodischarge

Table 4.4 shows the calculated discharge from 'best interpretation' paleogeometry values for each GPR line using Manning's Equation and Law of the Wall. Error is presented in Table 4.5, which shows instrumental error; and in Table 4.6 which presents a range based on potential maximum and minimum dimensions for each site. Based on the GPR and coring data, the paleochannels are most likely underestimated, not overestimated, due to lack of channel forms in subsurface within the designated paleochannel. However, minimums are presented where possible. The absolute maximum

possible paleochannel is represented by the surface expression viewed from lidar, and those were already determined to be too big to represent bankfull channels.

Estimations needed to be made for specific variables in order to calculate paleodischarge. Factors that were estimated to calculate mean velocity include roughness, slope, and hydraulic radius. Roughness is a hard variable to estimate in current river conditions, yet it has a strong influence on discharge calculations. For Manning's equation, the Manning's *n* value encompasses all factors that could impact the flow of water, including vegetation, bedforms, obstructions, etc. Whereas, the z_0 roughness term in the Law of the Wall only includes grain roughness. We completed a sensitivity analysis of roughness values to show the effect of varying Manning's *n* values between +/- 0.01 from the modern channel estimated roughness of n = 0.035 (http://www.fsl.orst.edu/geowater/FX3/help/8_Hydraulic_Reference/Mannings_n_Tables.htm). These variations fall within the range of error from instrumental error.

Using the current riverbed as an analog allows for the best estimation of roughness. Law of the Wall roughness was estimated using the D_{50}. A D_{50} of 20 mm (Johnson, 2012; Belmont, pers. communication) resulted in a grain roughness (z_0) of 0.0007 m. Variations in both grain roughness and Manning's *n* values, affect the estimated discharge.

Although slope changes are possible throughout the river's history, for this study, the current river was used as an analog for the paleochannels. Slope measurements were obtained from field data located near each paleochannel (Belmont pers. communication, 2015). The local slope applied to the paleodischarge calculations is 0.0012 for all

paleochannels. Finally, the hydraulic radius was calculated from the identified paleochannel boundaries and the modern hydraulic radii were taken from 2015 field data measurements (Belmont, pers. communication).

Table 4.4. Estimated discharge with Manning's Equation and Law of the Wall.

Line	Discharge Manning's n=0.035 (m^3/s)	Discharge Law of the Wall (m^3/s)
LS01A	**28**	52
LS01B	**58**	103
LS03A	**14**	11
LS03B	**17**	12
LS03C	**21**	15
LS05A	**82**	57
LS05B	**10**	6
LS05C	**15**	11
LS06A	**13**	9
LS06B	**26**	17
LS06C	**30**	23
LS01 modern	**155**	307
LS03 modern	**311**	614
LS05,6 modern	**275**	541

Table 4.5. Uncertainty in discharge due to instrumentation error.

Line	Width (m)	Avg. Depth (m)	Velocity (m/s)	Discharge (m^3/s)	Uncertainty from Instrumentation Error (± m^3/s)
LS01A	30	0.9	0.98	26	15
LS01B	34	1.3	1.28	57	23
LS03A	15	1	0.97	15	7
LS03B	16	1	1.01	16	8
LS03C	17	1.1	1.08	20	9
LS05A	30	1.7	1.48	75	24
LS05B	14	0.8	0.9	10	6
LS05C	17	0.9	0.96	15	8
LS06A	15	0.9	0.9	12	7
LS06B	19	0.9	1.23	21	12
LS06C	19	1.2	1.15	26	11

Table 4.6. Range of discharge determined from identifying alternate channel boundaries where applicable.

Line	Range of Discharge (m3/s)
LS01A	6-28
LS01B	56
LS03A	5-38
LS03B	17
LS03C	11-21
LS05A	38-82
LS05B	2-21
LS05C	5-15
LS06A	6-13
LS06B	26
LS06C	29

Paleodischarge estimated from surface expression via lidar are presented in Table 4.7. They represent the absolute maximum; however, based on the paleochannel to paleofloodplain ratio and the current channel to current floodplain ratio, it was concluded that the surface expression is indicative of the paleofloodplain rather than the paleochannel.

Table 4.7. Discharge estimated from combination of surface expression and GPR. GPR was used to determine maximum depth to till.

Site	Channel form from surface expression (m)	Approx. depth to till (m)	Estimated X-sect Area (m^2)	Manning's Discharge (m^3/s) n=0.035
LS01A	135	3	405	264
LS01B	95	3	285	186
LS01C	92	2.5	230	133
LS02A	188	2.3	423	227
LS02B	174	5	870	796
LS02C	182	3	546	355
LS03A	177	3.5	620	447
LS03B	235	3	705	459
LS03C	264	4	1056	833
LS05A	118	2.5	295	170
LS05B	85	3.5	298	215
LS05C	88	2.5	220	127
LS06A	65	3	195	127
LS06B	71	3	213	139
LS06C	75	3	225	146

In order to determine which method (Law of the Wall vs. Manning's equation) resulted in the most accurate estimation of velocity, and therefore discharge, these values were compared with estimated discharge from current channel geometries using the same methodology. These values were then compared with 1.5 and 2-year flood discharges calculated from a flood frequency analysis at the Red Jacket gage (USGS #05320500). Using the complete record, results show that Manning's proposed similar calculated discharge to the flood frequency analyses, validating the calculations (Table 4.8). Law of the Wall calculations doubled the estimated discharge for Le Sueur Sites 1, 3, 5 and 6 to 307 m^3/s, 614 m^3/s and 541 m^3/s, respectively. Based on my calculations and comparing

to recorded data by the USGS at Red Jacket gage #05230500, the most reasonable discharge measurements are from the GPR 'best interpretation' profile with a Manning's *n* value of 0.035, which is comparable to current channel roughness.

Table 4.8. Comparison of estimated discharge for modern channel and calculated discharge from flood frequency analyses.

Le Sueur Site	Channel width (m)	Avg channel depth (m)	Manning's Discharge (m^3/s)	1.5 year flood discharge (m^3/s)	2 year flood discharge (m^3/s)
1	53.8	2.71	170	76	142
3	53.8	2.93	310	76	142
5	39.04	2.33	248	76	142
6	39.04	2.33	248	76	142

Table 4.9. Comparison of all estimated discharge values.

Site	Best interpretation (m^3/s)	Surface expression (m^3/s)	Modern bankfull (m^3/s)	Flood frequency 1.5 year (m^3/s)	Flood frequency 2 year (m^3/s)
LS01A	6-28	264	155	76	142
LS01B	56	186	155	76	142
LS03A	5-38	447	310	76	142
LS03B	17	459	310	76	142
LS03C	11-21	833	310	76	142
LS05A	38-82	170	274	76	142
LS05B	2-21	215	274	76	142
LS05C	5-15	127	274	76	142
LS06A	6-13	127	274	76	142
LS06B	26	139	274	76	142
LS06C	29	146	274	76	142

Based on the calculated ‘best interpretation’ paleodischarge values, including error, discharge estimates in all paleochannels are one to two orders of magnitude smaller than the modern channel. Looking at factors that represent relative age, such as height above channel and distance upstream, there is little to no relationship among relative location and paleodischarge. The relationship between paleodischarge and chronology will be looked at in further detail in the OSL chronology section.

Some relationships were noted. Sites further upstream have lower estimated paleodischarge values, which corresponds with their location in respect to the confluences with the Maple and Cobb Rivers, excluding site 1 which has a lower paleodischarge than expected. And, eliminating the surface expression paleodischarge, since it is representative of the paleofloodplain, all paleodischarge values are one to two orders of magnitude smaller than current discharge using the same methodology and comparing flood frequency analyses.

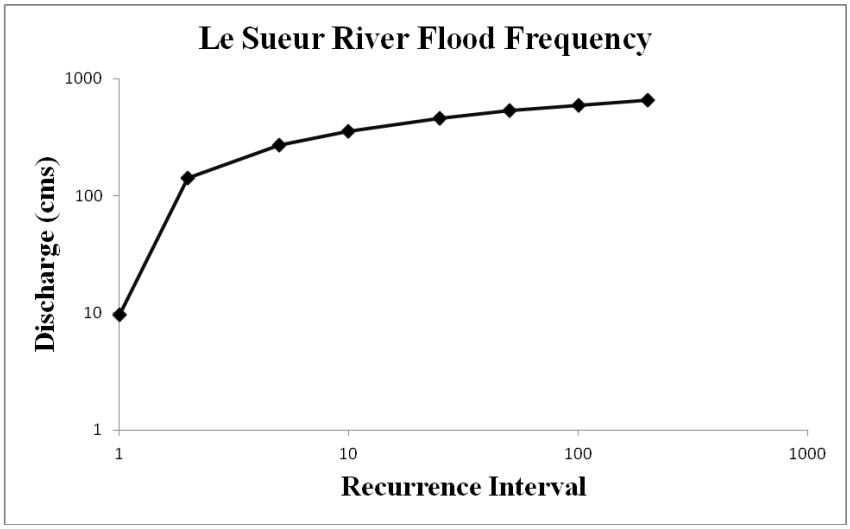

Figure 4.8. Flood frequency analysis for the Le Sueur River.

4.4 Historic channel development (1940-2013)

Historic aerial photography from 1949, 1950, 1964, 1991, 2003, and current river estimated widths, obtained from 2015 field data are presented in Table 4.11**.** Widths were measured within the knick zone, near Le Sueur Site 3. There is a linearly increasing width over time, suggesting there is also an increase in channel depth, assuming the b:h ratio is held constant.

Table 4.10. Estimated widths from aerial photos and September 2015 width from field measurements from within the knick zone.

Date	**Average Width (m)**
October 1949	13
August 1950	15
June 1964	33
April 1991	39
September 2003	42
Summer 2015	54

Channel geometry estimations show an increase in channel width, regardless of time of year. Increase from 1949 to 2003 in channel width suggests channels are widening (Table 4.10) and field surveys found measurable increases in width throughout the lower Le Sueur River from 2008 to 2015 (Belmont, pers. comm.). Incremental flood frequency analyses also show an increase in 1, 1.5, and 2-year floods throughout the record, first data point increases with the incremental periods, which is compatible with observations of increasing bankfull channel area over time (Figure 4.9; Table 4.11).

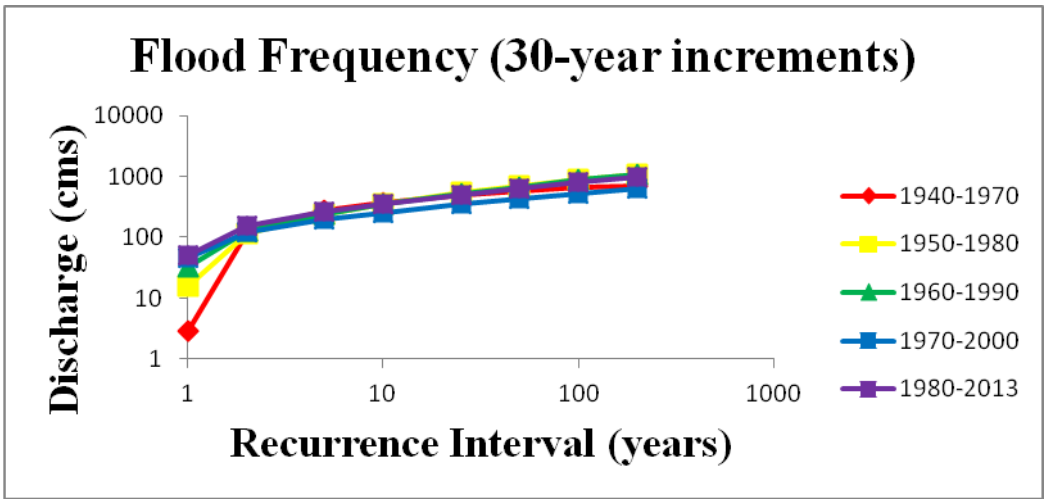

Figure 4.9. Incremental flood frequency analyses showing the trend in discharge over the 80-year data range.

Table 4.11. Table showing flood frequency increments and associated values for 1.5 and 2-year floods.

Increment of record	1.5 year flood (m^3/s)	2 year flood (m^3/s)
1940-1970	62	121
1950-1980	66	117
1960-1990	80	129
1970-2000	84	122
1980-2013	102	154

4.5 Chronology

OSL ages are provided in Table 4.12. Le Sueur Sites 3 and 5 fall around the time frame of the Mid-Holocene Dry Period (4 ka to 9 ka), however, there is no significant difference in discharge showing a signature for the MHDP. Table 4.13 and Figure 4.10 show the correlation between estimated age and discharge. Figure 4.10 shows that, even

with the most generous error included, there is a clear increase in discharge in the modern channel. Paleodischarge does not increase linearly.

Table 4.12. OSL data from Utah State University laboratory.

Site ID	USU Lab Number	Depth (m)	Number of aliquots	Dose Rate (Gy)	D_E[2] +/- 2σ	OD[3] (%)	OSL Age +/- 2σ
LS01	USU-1976	2.05	18(23)	2.58 +/- 0.12	24.45 +/- 2.79	15.9 +/- 4.0	9.48 +/- 1.41
LS03	USU1977	2.51	22(30)	1.97 +/- 0.09	15.58 +/- 2.43	27.7 +/- 4.9	7.92 +/- 1.45
LS05	USU-1978	1.72	15(22)	1.72 +/- 0.08	8.85 +/- 1.00	17.1 +/- 5.2	5.15 +/- 1.00
LS06	USU-1979	1.47	12(35)	1.76 +/- 0.08	4.65 +/- 1.06	35.6 +/- 8.7	2.64 +/- 0.65

Table 4.13. Range of discharges presented to represent each site along with the estimated age from OSL dating with associated error.

Site	Max Discharge (m^3/s)	Min Discharge (m^3/s)	Best Interpretation (m^3/s)	Age (ka)	Standard Deviation (ka)
LS01	58	6	28	9.48	1.41
LS03	38	5	17	7.92	1.45
LS05	82	2	21	5.15	1.00
LS06	29	6	26	2.64	0.65
2015	311	155	275	0	--

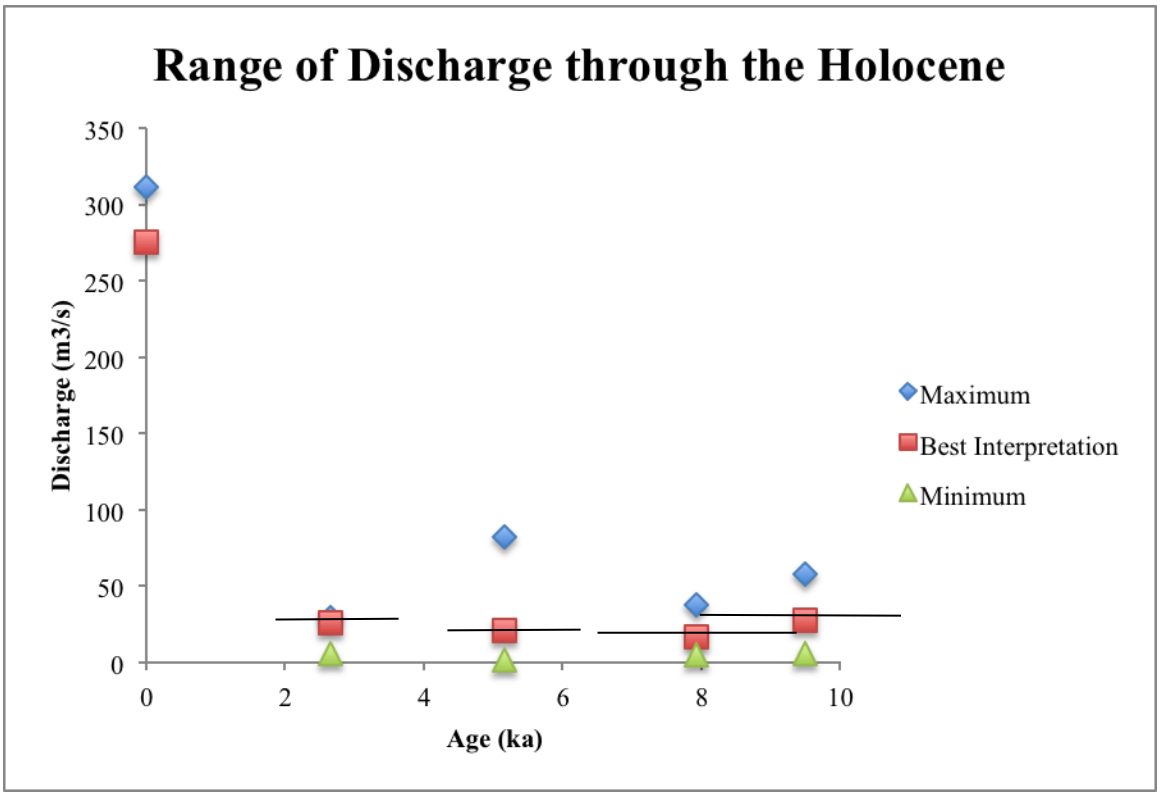

Figure 4.10. This shows the estimated maximum, best interpretation and minimum discharge values with OSL age included. Black bars represent error in OSL ages.

Section 5: Discussion

5.1 Discharge through the Holocene

The Le Sueur River basin has experienced perturbations on short and long timescales. When glacial Lake Agassiz drained, the resulting 70 m drop in base-level began a period of incision that is ongoing. Knickpoint migration upstream is characterized by steeper gradients, exposed bluffs and banks, and an expanding drainage network. Network expansion results in higher flows that erode banks and bluffs, bringing fine sediment into the system. Although climatic excursions, such as the Mid-Holocene Dry Period (MHDP) and Little Ice Age (LIA), may have an impact on discharge, this was not identifiable in the limited data presented here. We return instead to the competing hypotheses that discharge would increase steadily through the Holocene as drainage expanded vs. increasing rapidly in the past 200 years associated with land use change and more recently, climate change.

During the past 200 years, land use changes have altered the hydrology of the basin. Installation of tile drains and conversion from prairie to row-crop agriculture has affected the evapotranspiration rates and soil uptake of water, particularly in spring. This has routed more water to the river, increasing flows (Schottler et al., 2013). Although tile drainage coupled with drainage network expansion both lead to the hypothesis that discharge has increased from early Holocene to the present, the installation of ditches and tile drains rapidly integrated the drainage network, increasing the size of the watershed, and thus increasing discharge more rapidly than Holocene-scale drainage network expansion. The hypothesis that land use change would result in a stepped increase in

discharge with land use conversion would match depositional records in Lake Pepin (Engstrom et al., 2009) and erosional records determined from numerical modeling in the Le Sueur River basin (Gran et al., 2013). Paleodischarge estimations support this hypothesis, showing an increase post-settlement rather than a slow and steady rise over the Holocene.

It is most likely that channels have increased in size through time due to drainage network expansion and anthropogenic factors, however, an alternative hypothesis is that in the early Holocene, rivers in the area may have been significantly larger than present. For terraces that are around 11 ka (LS01), climate could have caused rivers to be larger through higher discharge associated with increased drainage from the Laurentide Ice Sheet. These channels could have a braided form, with higher different width-to-depth ratios. However, there was no braided channel signature identified from the data, leading to the conclusion that the channels were meandering. There is also no signature identifiable in the data provided of larger channels in the early Holocene. For the terraces around 6 ka (LS03, LS05 and LS06), drier climate would have led to channels that were likely smaller, which is consistent with the estimated paleogeometry, but not statistically significant within error. Determining the accuracy of the paleogeometry estimations will allow for a better understanding of paleodischarge values.

Over time, width-to-depth ratio should remain constant. Based on this understanding, paleodischarge estimated from surface expression is too large, and is best estimated using the ‘best interpretation’ paleogeometry from GPR data. This was

validated by mimicking the calculations done on the paleochannels and applying them to the modern channel, which we have field measurements.

Comparing the methodology for estimating paleodischarge, it was concluded that Manning's equation better estimated paleodischarge. It is assumed that the variations in values estimated from Manning's equation and Law of the Wall are due to the lack of roughness accounted for in Law of the Wall, which is why the discharge comes out to be almost double Manning's estimates. Roughness is very complicated to estimate and causes variation in calculated discharge.

In order to show just how sensitive discharge calculations are to roughness, I completed a sensitivity analysis. This resulted in approximately 10% change in estimated velocity. Although the current roughness was reasonable to use in this instance, if roughness varied in the past, then it would likely be much higher due to lack of anthropogenic impacts on the system which could include removing snags or straightening channels. However, the roughness sensitivity analysis fell within the instrumental error and therefore is accounted for in the instrumental error measurements. Instrumental error was accounted for and reached as high as 50% of the estimated discharge. This suggests that GPR in clay-rich environments can show large-scale details, but should not be used when attempting to identify fine features within the subsurface, such as channel bedforms.

Using the 'best interpretation' geometry and the discharge estimated using Manning's Equation with a roughness n of 0.035, it is clear there has been a significant increase in discharge through the Holocene, with most of that increase happening since

the youngest terrace studied. The largest realistic 'best interpretation' paleochannel geometry indicates flows around 82 m^3/s. Using the smallest value for comparison on the modern river, the discharge was calculated at 155 m^3/s; an increase of a factor of two. Thus, a conservative estimate suggests that the measured paleochannels are at least a factor of 2 smaller than the modern channel estimations.

Flood frequency analyses suggest an increase in discharge throughout the record. The whole record estimated a 1.5 and 2-year flood of 76 m^3/s and 142 m^3/s, respectively, Incremental flood frequency analyses show a steady increase in discharge over the past 80 years, with the last increment (1980-2013) estimating 1.5 and 2-year floods at 102 m^3/s and 154 m^3/s, respectively (Table 5.1). This is supported by evidence of increasing channel width seen in historical air photos.

Table 5.1. Comparison of paleodischarge estimations using all methods, modern bankfull estimated from field measurements, and flood frequency 1.5- and 2-year flood discharges from the last increment (1980-2013).

Site	Best interpretation (m^3/s)	Surface expression (Interpreted as Floodplain) (m^3/s)	Modern bankfull (m^3/s)	Flood frequency 1.5 year (m^3/s)	Flood frequency 2 year (m^3/s)
LS01A	19-28	264	155	102	154
LS01B	58	186	155	102	154
LS03A	14-121	447	310	102	154
LS03B	17	459	310	102	154
LS03C	21	833	310	102	154
LS05A	36-82	170	274	102	154
LS05B	10-121	215	274	102	154
LS05C	5-57	127	274	102	154
LS06A	13-16	127	274	102	154
LS06B	20-26	139	274	102	154
LS06C	30	146	274	102	154

Uncertainties in the paleogeometry estimates result in a range of paleodischarge values for all sites, and the values for LS03, LS05 and LS06 are not significantly different from LS01. We would expect them to be smaller; however, this is not discernible with the low precision of the GPR interpretation. The Maple and Cobb Rivers enter the Le Sueur River downstream of LS05 and LS06, which suggests the paleodischarge should be smaller at sites located upstream of the confluences.

Overall, we have evidence that shows the Le Sueur River has incised and widened, increasing the discharge in the river over time (Gran et al., 2009), but no studies have been done to quantify the magnitude of the increase or whether it is comparable to documented increases in sediment loading to Lake Pepin (10-fold). Based on these

results, there was an increase of at least 2 times the discharge through the late Holocene as preserved in the paleochannels. This corresponds well with the increase in fine-sediment loading seen in Lake Pepin. A previous study in the Le Sueur found only a 3-fold increase in valley erosion rates, where the model used to determine this used a constant discharge and modern channel geometry. In order to accurately model and estimate changes in sediment flux through time, we need to have a constraint on changes in discharge. Discharge is directly related to erosion, and therefore, estimating paleodischarge will aid in modeling efforts throughout the Le Sueur River and the GBER basin.

There are many limitations when estimating paleogeometry with GPR, including GPR data collection, estimating paleogeometry from the GPR profiles, the possibility that coarse gravel does not represent the base of channel, and that the preserved channel is not actually representative of the paleochannel. The calculation methods appear valid based on reconstruction of modern discharge from channel geometry, thus most of the error comes in estimating geometry and channel roughness. This technique could be improved by coring at more locations along the line and using several different frequencies of GPR antennae. In addition, one of the underlying assumptions is that the paleochannel slope has not changed through the process of preservation, which may not be valid.

5.2 Meandering river preservation

This study involved using GPR to image paleochannel cross-sections preserved in the subsurface to obtain paleogeometry. This led to questions about meandering river preservation. One of the premises of this study is that cut-off meanders will be preserved

in the subsurface as a filled-in channel, with the original geometry preserved (cut bank on one side, point bar on the other; Figure 5.1). In order to preserve paleochannel geometry, the meander bend must be cut off from the river. If the channel was migrating laterally, then the channel form will be lost; however, when the channel is cut-off, lateral migration ceases, and the channel is preserved (Lewin and Macklin, 2003). In the Le Sueur River, incision has resulted in stranded paleochannels preserved on terraces as cut-off meanders throughout the basin, suggesting there should be an identifiable paleochannel. Once the meander is stranded, it will fill in. Throughout the study area, all outside factors (climate, geology, land use) are the same; however, paleochannel infilling occurred several ways. Processes of infilling determine how the channel will be preserved. None of the GPR profiles show a cutbank/point bar geometry as would be expected; instead, there were indications of several different filling processes (figure 5.2):

- Overbank deposition of fine sediment
- Lateral accretion of bedforms
- Downstream migration of bedforms

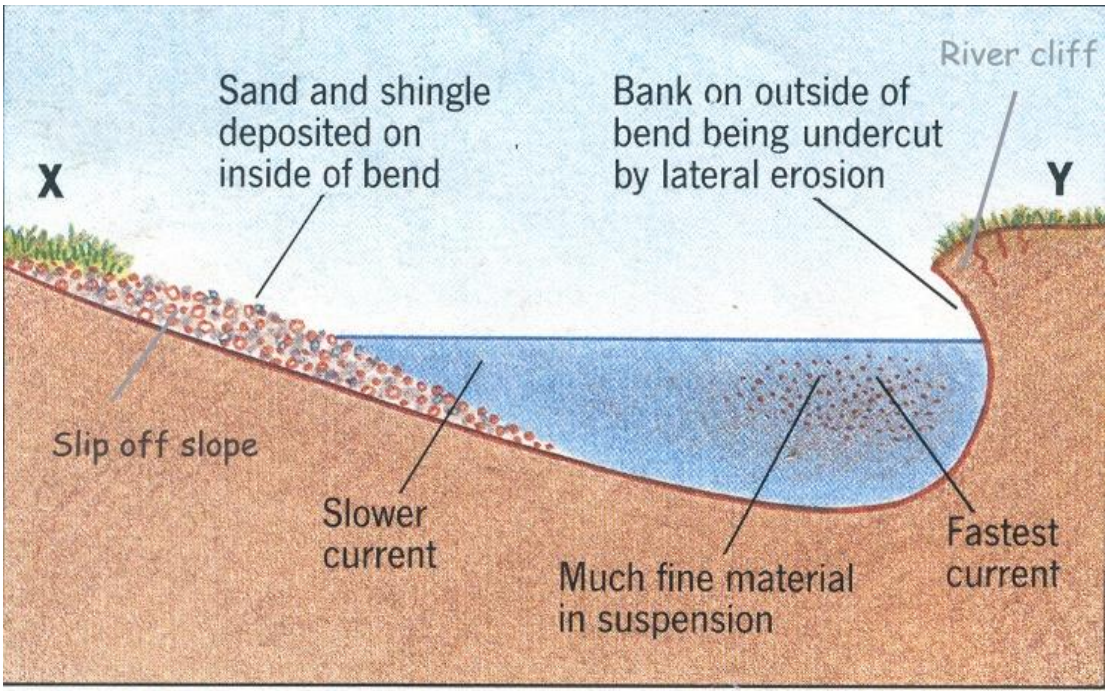

Figure 5.1. This is a cartoon version of a meandering river channel, which should be preserved in the sub-surface. (from www.coolgeography.co.uk)

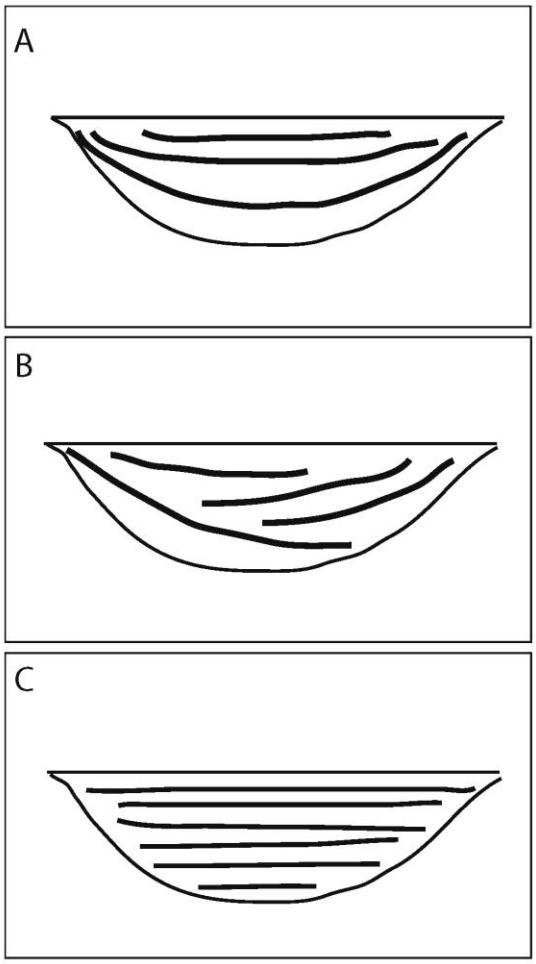

Figure 5.2. The above diagram shows the different ways sediment filled in the abandoned meander cutoffs. Diagram A represents overbank deposition of fine sediment, B represents lateral accretion of bedforms, and C represents downstream migration of bedforms.

Figure 5.2 shows the layout of sediment packages representing different infilling processes. Part A shows the overbank deposition of fine sediment, B shows the lateral accretion of bedforms, and C shows downstream migration of bedforms. Overbank deposition of fine sediment occurs when water levels rise high enough to force smaller

particles to settle within the floodplain; lateral accretion of bedforms occurs when forms similar to point bars laterally migrate across the channel, filling it in; and downstream migration is fundamentally the same as lateral accretion but with bar forms migrating in a different orientation. It is also possible for several of these processes to occur at once. The collected GPR profiles show that all 3 processes occurred within the Le Sueur River basin. For example, line LS03B shows overbank deposition, line LS01B shows lateral accretion, and line LS05A shows downstream migration.

Erskine et al. (1992) determined that infill is characterized by several factors (sediment availability, frequency of transporting flows, and variability in deposition within a single cutoff) and suggest there should not be a universal model for alluvial cutoff infills. The Le Sueur River is currently experiencing an incision event, which should be expected to result in better preservation of channel geometry, but perhaps less fill overall. Variations within the watershed result in different processes filling in meander cut-offs. The sites studied in this project further validate the hypothesis that no universal model should be used to describe all meander cut-offs filling in. An attempt can be made at estimating paleochannel geometry, but caution must be taken. This channel *could* represent the paleochannel, but has likely been altered through the process of infilling.

5.3 Future work

GPR profiling is a useful tool for estimating paleogeometry, however, there are several factors that impact the quality of the data, including sediment type and water content. In order to estimate channel geometry correctly, cores must be taken. It has been

reported, and these data further validate, that the preservation of meandering rivers in the subsurface is complicated and could represent the past channel form or smaller channels that were occupied. These complications create a wide range of uncertainty within the calculations. Therefore, if a similar study is to be conducted, I suggest using various antennae frequencies and an abundance of cores to help identify channel boundaries. This is due to fine sediments and their high dielectric permittivity attenuating the signal., and the difficulty associated with correctly estimating channel geometry.

During data collection, I also collected samples for OSL dating on terraces within the Blue Earth River to expand work on valley and channel evolution into the neighboring Blue Earth River Basin. I collected 13 samples from terraces of varying height above channel and distance upstream from the confluence with the MN River to create spatial and temporal variation within the data (Appendix III). Samples will be used to look at river incision through time to create an incision history for the Blue Earth River to compare with the Le Sueur River evolution model (Gran et al., 2013).

Section 6: Conclusion

Base-level drop in the Minnesota River Basin has caused geomorphic adjustments of the rivers. The knickpoint, which is propagating upstream, translating the new base-level to the rest of the watershed, has increased slopes and erosion rates as higher flows remove fine sediment from banks and bluffs. Higher flows are the result of both drainage network expansion over the Holocene and the more recent land cover changes and installation of surface and subsurface drainage in the last 200 years. Obtaining paleogeometry of meander bends preserved on terraces coupled with chronologic techniques allow for the reconstruction of the Le Sueur River's discharge history.

Incorporating uncertainty can potentially change the estimated paleodischarge by 150%. Based on the data, paleodischarge estimated from 'best interpretation' geometry and velocity measurements using Manning's equation with a roughness of 0.035 results in the most realistic paleodischarge values. The primary concern when completing these estimations is the interpretation of river channel geometry preserved in the subsurface. Meander bend cut-offs are preserved in the sub-surface through a balance of sediment availability, frequency of transporting flows, and variability in deposition within a single cutoff. It has been resolved that a universal model for alluvial channel fill-in would not be appropriate, and my study validates this argument. Although my sites are located within the same environment geologically, several different processes have filled in the paleochannels including overbank deposition, lateral accretion, and downstream migration. Different processes result in different packages within the paleochannel fill and complicate estimating channel boundaries. Overall, although GPR is a valuable tool,

it was challenging to interpret in fine sediments; increasing the number of sediment cores could increase the confidence in estimating channel boundaries.

Paleogeometry and paleodischarge measurements suggest minimal variations over the Holocene with more pronounced changes to the river channel since the time of paleochannel abandonment. Although there are no trends identified within the paleodischarge values at the Le Sueur River sites during the Holocene, using ‘best interpretation’ estimations, there has been an increase of a factor of 2 between the time of paleochannel abandonment and current river conditions.

References

Ankjærgaard, C., Guralnik, B., Porat, N., Heimann, A., Jain, M. and Wallinga, J., 2015. Violet stimulated luminescence: geo-or thermochronometer? *Radiation Measurements*, *81*, pp.78-84.

Bartlein, P.J., Webb III, T., and Fleri, E., 1984. Holocene Climatic Change in Northern Midwest: Pollen-Derived Estimates. *Quaternary Research* **22:** 361-374.

Belmont, P., Gran, K.B., Schottler, S.P., Wilcock, P.R., Day, S.S., Jennings, C.J., Lauer, J.W., Viparelli, E., Willenbring, J.K., Engstrom, D.R., Parker, G., 2011a. Large shift in source of fine sediment in the upper Mississippi River. *Environmental Science and Technology* **45**(20): 8804-8810.

Belmont, P., Gran, K., Jennings, C.E., Wittkop, C., Day, S.S., 2011b, Holocene landscape evolution and erosional processes in the Le Sueur River, central Minnesota, *in* Miller, J.D., Hudak, G.J., Wittkop, C., and McLaughlin, P.I., eds., *Geological Society of America Field Guide* 24.

Bevis, M., 2015. *Sediment budgets indicate Pleistocene base level fall drives erosion in Minnesota's greater Blue Earth River basin*. M.S. Thesis: University of Minnesota Duluth, 89 p., http://hdl.handle.net/11299/170661.

Blann, K.L., Anderson, J.L., Sands, G.R. and Vondracek, B., 2009. Effects of agricultural drainage on aquatic ecosystems: a review. *Critical reviews in environmental science and technology*, *39*(11), pp.909-1001.

Bristow, C.S., and Jol, H.M., 2003, Ground penetrating radar in sediments: *Geological Society special publication* 211, 330 p.

Clayton, L and Moran, SR, 1982, Chronology of late-Wisconsinan glaciation in middle North America: *Quaternary Science Reviews*, v. 1, p. 55-82.

Day, S.S., Gran, K.B., Belmont, P. and Wawrzyniec, T., 2013. Measuring bluff erosion part 1: terrestrial laser scanning methods for change detection. *Earth Surface Processes and Landforms*, *38*(10), pp.1055-1067.

Erskine, W., McFadden, C. and Bishop, P., 1992. Alluvial cutoffs as indicators of former channel conditions. *Earth Surface Processes and Landforms*, *17*(1), pp.23-37.

Engstrom, D.R., Almendinger, J.E., Wolin, J.A., 2009. Historical changes in sediment and phosphorus loading to the upper Mississippi River. *Journal of Paleolimnology* **41**(4): 563-588.

Gran, K.B., Belmont, P., Day, S.S., Jennings, C., Johnson, A., Perg, L., and Wilcock, P.R., 2009, Geomorphic evolution of the Le Sueur River, Minnesota, USA, and implications for sediment loading, *in* James, L.A., Rathburn, S.L., and Whittecar, G.R., eds., *Management and restoration of fluvial systems with broad historical changes and human impacts*: Geological Society of America Special Paper 451, p. 119-130.

Gran, K.B., Belmont, P., Day, S.S., Jennings, C., Lauer, J.W., Viparelli, E., Wilcock, P.R., and Parker, G., 2011a, *An integrated sediment budget for the Le Sueur River basin: Final Report to the Minnesota Pollution Control Agency*, 119 p.

Gran, K.B., Finnegan, N., Johnson, A.L., Belmont, P., Wittkop, C., and Rittenour, T., 2013, Landscape evolution, valley excavation, and terrace development following

abrupt postglacial base-level fall, *Geological Society of America Bulletin*, doi: 10.1130/B30772.1.

Hancock, G.S, and Anderson, R.S., 2002, Numerical modeling of fluvial strath-terrace formation in response to oscillating climate: *Geological Society of America Bulletin*, v. 114, p. 1131-1142.

Indiana Department of Natural Resources, 1996. Section 5.2: Tile Drain Installation and Repair.

Jennings, C.E., 2007, Overview of the Quaternary geologic history of the Minnesota River, chapter 2 *of* Native plant communities and rare species of the Minnesota River valley counties: Minnesota County Biological Survey, Division of Ecological Resources, Minnesota Department of Natural Resources, Biological Report No. 89.

Jol, H.M. and Bristow, C.S., 2003. GPR in sediments: advice on data collection, basic processing and interpretation, a good practice guide. *Geological Society, London, Special Publications, 211*(1), pp.9-27.

Jol, H.M., 2009, *Ground Penetrating Radar: Theory and Applications*, Elsevier, United Kingdom, 524 p.

Kelley, D.W., and Nater, E.A., 2000, Historical sediment flux from three watersheds into Lake Pepin, Minnesota, USA: *Journal of Environmental Quality,* v. 29, n. 2, p. 561-568.

Knox, J.C., 1993, Large increases in flood magnitude in response to modest changes in climate. *Letters to Nature* v. 361: 430-432.

Knox, J.C., 2000. Sensitivity of modern and Holocene floods to climate change. *Quaternary Science Reviews* v. 19, p. 439-457.

Knox, J.C., 2001. Agricultural influence on landscape sensitivity in the Upper Mississippi River Valley. *Catena* v. 42, p. 193-224.

Lewin, J. and Macklin, M.G., 2003. Preservation potential for Late Quaternary river alluvium. *Journal of Quaternary Science*, *18*(2), pp.107-120.

Lusardi, B.A., 1994, Minnesota at a Glance: Quaternary Glacial Geology. University of Minnesota.

Madsen, A.T., and Murray, A.S., 2009, Optically stimulated luminescence dating of young sediments: A review, *Geomorphology* 109, p. 3-16.

Mayewski, P.A., Rohling, E.E., Stager, J.C., Karlén, W., Maasch, K.A., Meeker, L.D., Meyerson, E.A., Gasse, F., van Kreveld, S., Holmgren, K. and Lee-Thorp, J., 2004. Holocene climate variability. *Quaternary research*, *62*(3), pp.243-255.

Miao, X.D., Mason, J.A., Goble, R.J., and Hanson, P.R., 2005, Loess record of dry climate and eolian activity in the early to mid-Holocene, central Great Plaines, North America: The Holocene, v. 15, p. 339-346, doi: 10.1191/0959683605h1805rp.

Marschner, F.J., 1930, Interpretation of Francis J. Marschner's map of the original vegetation of Minnesota: Based on notes of the Public Land Survey, 1847-1907.

Minnesota Climatology Working Group, State Climatology Office - DNR Division of Ecological and Water Resources, University of Minnesota, 2014. Historical Climate Data Retrieval. climate.umn.edu/doc/historical.htm

Minnesota Department of Natural Resources, 1988. Minnesota Early Settlement Vegetation (digitized map). Accessed September 2014.

Minnesota Historic Farms Study (No date). Developmental periods in the historic context "Euro-Americans farms in Minnesota, 1820-1960" [online]. Available at http://www.dot.state.mn.us/culturalresources/pdf_files/crunit/devperiods.pdf (May 2014).

Minnesota Pollution Control Agency (MPCA), Minnesota State University Mankato Water Resources Center, 2011, Turbidity Total Maximum Daily Load Study, Greater Blue Earth River Basin.

Novotny, E.V. and Stefan, H.G., 2007, Stream flow in Minnesota: Indicator of climate change: *Journal of Hydrology* (Amsterdam), v. 334, p. 319-333, doi: 10.1016/j.jhydrol.2006.10.011.

Olley, J., Caitcheon, G., Murray, A., 1998, The distribution of apparent dose as determined by optically stimulated luminescence in small aliquots of fluvial quartz: implications for dating young sediments, *Quaternary Geochronology*, v. 17, p. 1033-1040.

Ritter, D.F., Kochel, R.C., Miller, J.R., 2006, *Process Geomorphology,* Waveland Press, Long Grove, IL, 560 p.

Sambrook Smith, G.H., Ashworth, P.J., Best, J.L., Woodward, J. and Simpson, C.J., 2006. The sedimentology and alluvial architecture of the sandy braided South Saskatchewan River, Canada. *Sedimentology*, *53*(2), pp.413-434.

Schottler, S.P., Ulrich, J., Belmont, P., Moore, R., Lauer, J., Engstrom, D.R. and Almendinger, J.E., 2014. Twentieth century agricultural drainage creates more erosive rivers. *Hydrological processes*, *28*(4), pp.1951-1961.

Teller, J.T., Thorleifson, L.H., Matile, G. and Brisbin, W.C., 1996. Sedimentology, geomorphology and history of the central Lake Agassiz Basin. Field Trip Guidebook B2. *Geol Assoc of Canada/Minerol Assoc of Canada, 84*.

Thorleifson, L.H., 1996, Review of Lake Agassiz history *in* J.T. Teller, L.H. Thorleifson, G. Matile and W.C. Brisbin, 1996, Sedimentology, Geomorphology and History of the Central Lake Agassiz Basin - Field Trip Guidebook B2; Geological Association of Canada/Mineralogical Association of Canada Annual Meeting, Winnipeg, Manitoba, May 27-29, 1996.

Thorleifson, L.H., Jirsa, M.A., Boerboom, T.J., Chandler, V.W., Mossler, J.H., Runkel, A.C., Setterholm, D.R., 2011, Geologic Map of Minnesota Bedrock Geology. State Map Series S-21. *The Minnesota Legislature as Administered by the Minerals Coordinating Committee.*

Wallinga, J., 2002, Optically stimulated luminescence dating of fluvial deposits: a review, *Boreas,* v. 31, p. 303-322. Oslo. ISSN 0300-9483.

Water Resources Center, Minnesota State University, Mankato, 2000, Le Sueur River major watershed diagnostic report: Le Sueur River basin implementation framework, MPCA Clean Water Partnership Project #951-1-1-194107, 162 p.

Wegmann, K.W. and Pazzaglia, F.J., 2002, Holocene strath terraces, climate change, and active tectonics: The Clearwater River basin, Olympic Peninsula, Washington State: *Geological Society of America Bulletin* 114, p. 731-744.

Winkler, M.G., Swain, A.M. and Kutzbach, J.E., 1986. Middle Holocene dry period in the northern Midwestern United States: lake levels and pollen stratigraphy. *Quaternary Research*, *25*(2), pp.235-250.

Appendix I—GPR line descriptions and interpretations

Images have been processed in Ekko Project 2 following same methodology described in methods section. Where applicable, maximum and/or minimum channel boundaries were identified; blue lines representing minimum dimensions and orange lines representing maximum dimensions.

LS01A—Start of line (0 m) has set of reflections that are sub-horizontal and discontinuous (maybe erosional). At 14 m, there are semi-continuous reflections that have a concave down shape (dome). This continues until 34 m, where the reflections begin to flatten out to horizontal to sub-horizontal., but are still semi-continuous. At 54 m, reflections start to dip toward the end of the line, still semi-continuous. Dipping in gentle and increases slope as depth increases. At this same location, depth of penetration increases from 4 meters to approx. 6 meters. Reflections on top of the dipping reflections are hummocky and sub-horizontal (infill). This continues to the end of the line.

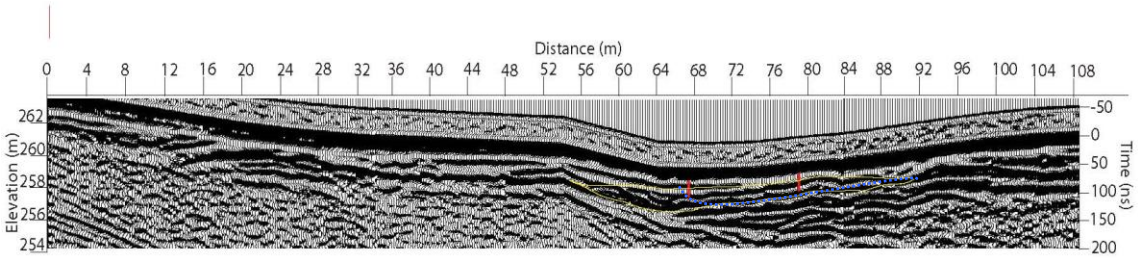

LS01B—I love this line; it is very clear what I am looking at. At start of line (0 m), there are several horizontal., continuous reflections that are truncated by steeply-dipping reflections. Dipping is towards the end of the line and slope increases with depth. Within concave up shape, there are gently-dipping to sub-horizontal reflections. Concave up shape spans 20-50 meters (roughly). Depth of penetration is much greater at the beginning of the line (up to 30 meters). It starts at 4 meters and decreases to about 2 meters. At 52 meters, reflections are still gently-dipping towards concave up shape, but are starting to flatten out. Reflections are hummocky throughout the line with little undulations. At the very end of the line there are air waves present at depth.

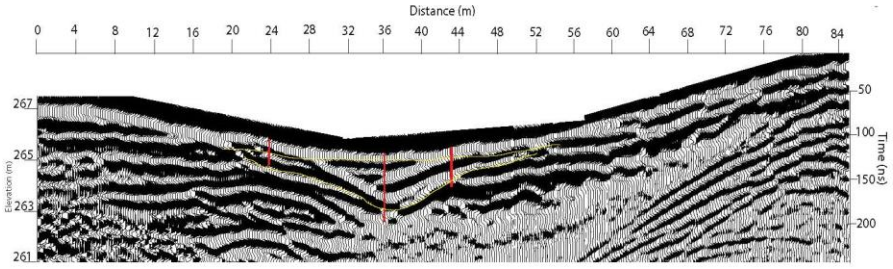

LS03B—Located closest to LS River on this site. From start (0 m), gently-dipping, semi-continuous reflections that have a convex up shape from 8- 10 meters with underlying reflections following the same pattern. At 14 meters, depth of penetration increases and I can see a boundary between 2 units with very little visible below. At 15 meters, reflections start to dip towards the convex up shape and appear to be foresets. Reflections are hummocky and appear to mainly be dipping towards the convex up shape. Towards 40 meters, uppermost reflections appear to flatten out and become sub-horizontal. All reflections appear to be semi-continuous. At 52 meters, there is another set of reflections that is dipping (very gently), which is then cut off by a set of reflections dipping the opposite direction at a much greater slope, ranging from 56 to 65 meters. At the end of the line, the reflections are nearly horizontal., however, they are not continuous.

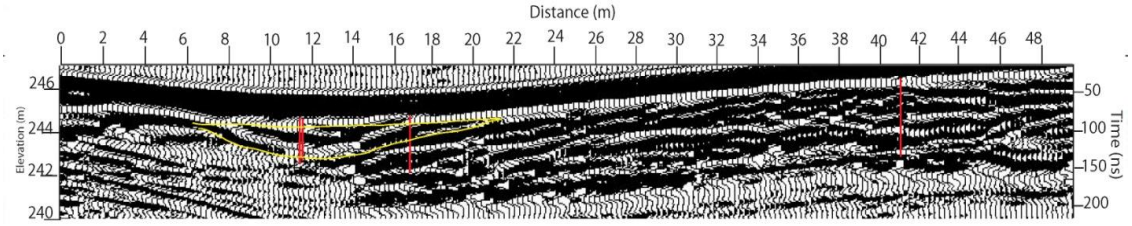

LS03C—semi-continuous reflections that are sub-horizontal from the start and following the slope of the ground surface. There are hummocks found within the first 50 meters, and there are air waves starting at 3 m depth and continuing to the base of the line. Reflections do not penetrate deep and seems to be marked by a boundary between 2 units. For the next 50 meters, there is little penetration and the reflections that are seen are sub-horizontal and semi-continuous. At around 86 m, the upper reflection fades into the one underlying it. At 100 meters, there is a gently-dipping bed that dips toward the start of the line. Around 110 meters (roughly), depth of penetration increases drastically and marks the boundary between 2 units at around 6 meters depth. Reflections are semi-continuous, hummocky, and range from sub-horizontal to gently-dipping. Gently-dipping reflections range from 104-114 meters. Between 100 and 200 meters, the line becomes very complex. There are packages of gently-dipping reflections going in both directions. Some steeply-dipping reflections are present at 136-146 meters that are truncated by sub-horizontal reflections above. The entire section has hummocky reflections that are semi-continuous and sub-horizontal. Areas with gently-dipping reflections are different in terms of dip direction and angle. The last 20 meters of the line are characterized by gently-dipping reflections that peter out and flatten. These are also semi-continuous.

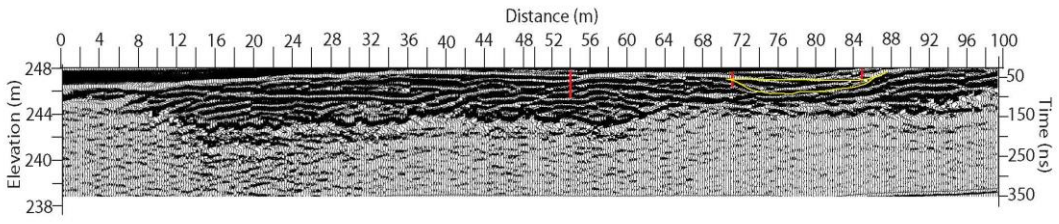

LS05A—At start of line (0 m), reflections are semi-continuous and sub-horizontal with the ground surface. There appear to be some hummocks, but unsure if this is just noise. At approx. 20m, reflections steeply-dip away from start and gradually flatten out as move up in depth. When following the steeply-dipping reflections, depth of penetration decreases and the reflections are cut off. Within this area that is very shallow, the upper reflections are sub-horizontal. Below, there is a very faint reflection that mimics the same shape at the upper reflections, but it is unclear whether this is noise or an actual bed that is light due to loss of penetration. At the end of the line, there are air waves, but they are underlying sub-horizontal., semi-continuous reflections that very, very gently dip towards the start of the line.

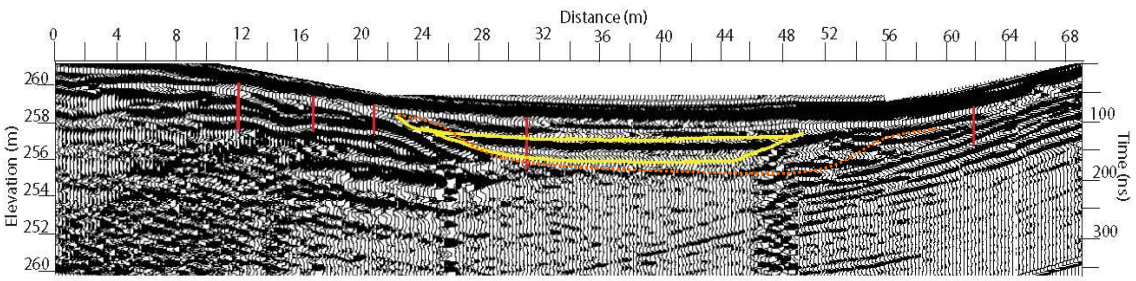

LS05B—Start of line (0 m), reflections are sub-horizontal and semi-continuous. At 20 m, reflections begin to dip towards the end of the line, but very gently. As depth increases, the steepness of those reflections increases (relatively small increase). This trend continues until about 30 meters, where the reflections begin to dip in the opposite direction. This results in a convex shape. Within the first 50 meters or so, there are some hummocky locations. Between 36 and 46 meters, there is a loss of penetration depth. At 48 m (approx.), reflections become continuous and horizontal. This trend continues until the end of the line. There is a little bit of noise within the reflections around 82 meters.

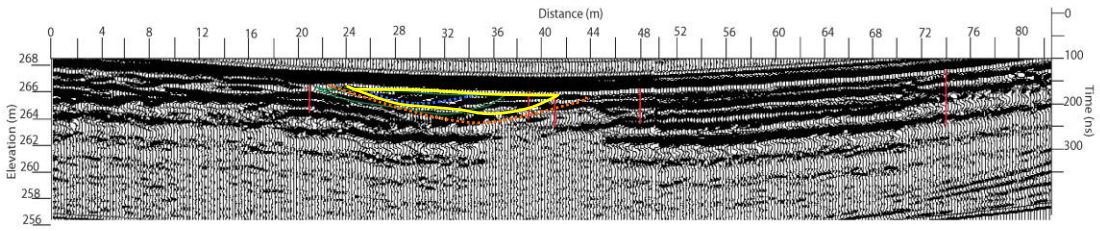

LS05C—Start of line (0 m), semi-continuous, sub-horizontal following the ground surface. Reflections are hummocky and depth of penetration reaches approx. 6 meters deep (indicating amount of fines in deposits). At 40 meters, reflections are gently-dipping toward the end of the line. Then, the depth of penetration decreases to about 4 meters. From 42 meters to 60 meters (approx.), there is a slight concave up shape, but all of the reflections do not continue due to loss of penetration depth. Small and less obvious concave up shapes appear within the larger shape (infill). From 60-90 meters, the reflections are gently-dipping towards the start of the line. They are semi-continuous and dipping flattens out towards the end where the reflections become sub-horizontal with the ground surface again.

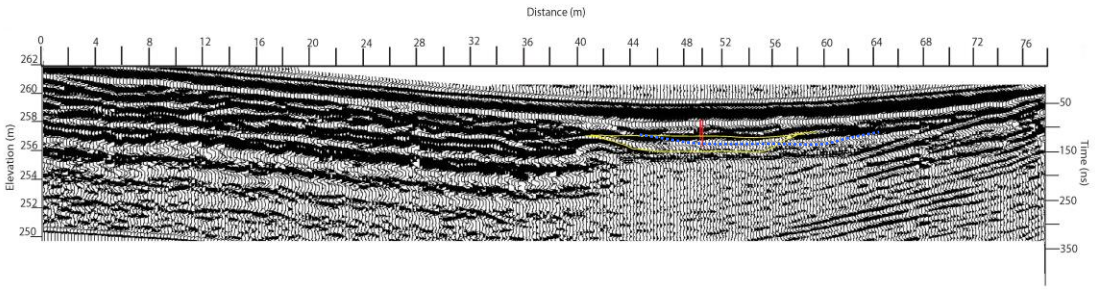

LS06A—Start of line (0 m) has semi-continuous to continuous, slightly dipping reflections. Reflections are hummocky within the first 40 meters, and then the signal becomes attenuated. Signal penetrates deeper in the beginning of the line and loses detail between 44 m and 60 m approximately. Steeply dipping reflections near the end of the line, represent air waves and are noise in the data.

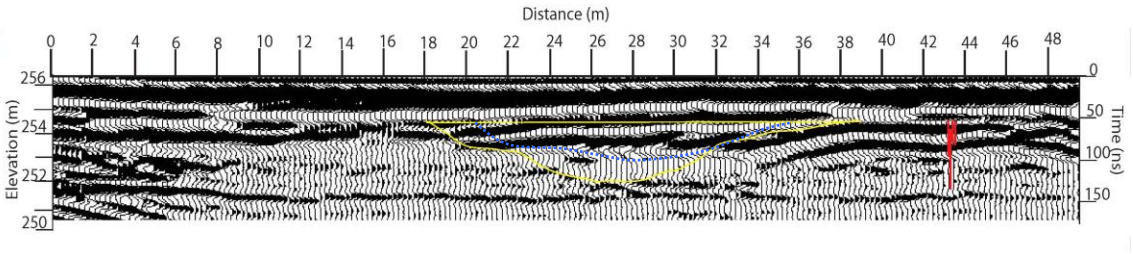

LS06B—Start of line (0 m), semi-continuous, sub-horizontal following the ground surface. Reflections are slightly hummocky and depth of penetration reaches approx. 6 meters. In general., reflections are sub-horizontal to horizontal.

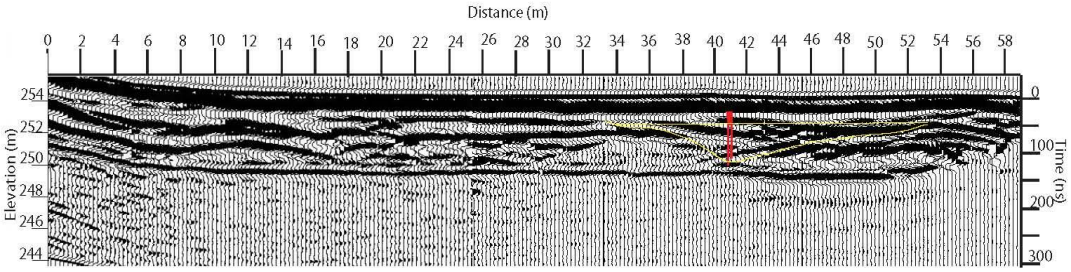

LS06C—Start of line (0 m), semi-continuous, sub-horizontal following the ground surface. Reflections are hummocky and depth of penetration reaches approx. 6 meters. There is a dark reflection approx. 4 meters below surface that continues across the entire line. Above this reflection, there are hummocky, semi-continuous reflections that span the entire line. There are also reflections that show 2 directions of filling in (between 16 and 20 m; between 38 and 46 m).

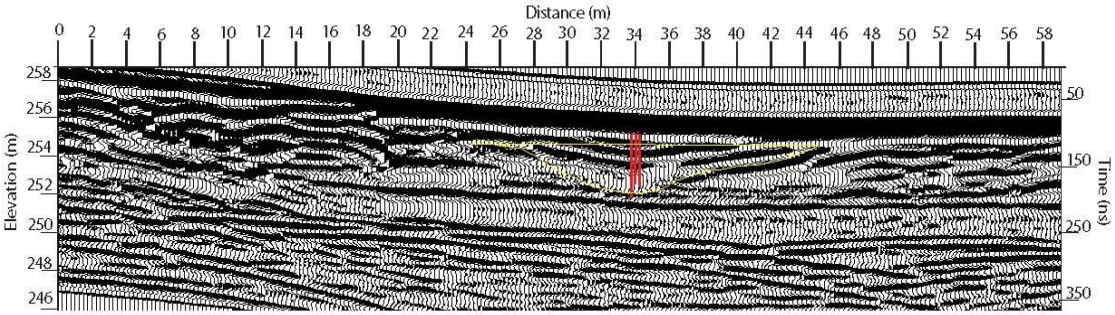

Appendix II—Optically Stimulated Luminescence data processing:

Here are directions for sample prep of OSL sample.

In addition to paleochannel discharge analysis on the Le Sueur River, I hope to extend our understanding of valley evolution from the Le Sueur to the GBER basin. The Holocene timescale of the GBER basin will be studied through the collection of samples for OSL dating on terraces. Terraces of varying heights and distances upstream will be dated to better grasp the natural response of the river to changes in climate over this longer period. OSL dates will allow me to construct a database of channel change over the Holocene timescale, which will then be used by others to help inform modeling efforts.

From that point on, the sample would be referred to by its USU number. Once samples were logged in the processing book, the sample book, and the dose rate book, the sample (light-proof tube), water content, and dose rate needed to be labeled with the appropriate USU number. These 3 pieces of information are processed differently.

When taking a small portion of a larger sample, we tend to select what we think is the appropriate representative sample; this is incorrect. In order to get a proper sample that accurately depicts the total sample, a splitter needs to be used. A splitter is a metal contraption that has an opening at the top and 2 sets of chutes that lead to 2 different buckets. Once the buckets are filled, one is selected and then poured again. This is repeated, using the same bucket, until the sample is between 25 and 50 mL. The same process is used to archive some of the dose rate; the archived sample is between 150 and

250 mL. Once bagged, the sample is recorded on a datasheet being sent to the lab and the sample is tossed in the box.

Extracting the sample from the tube is done by wiping every surface down with DI water several times so there are no visible grains. Then, the sample tube, scoopula, and Kim Wipes are used to remove the outer 2 cm on each side of the tube. This sediment is placed in a beaker that is labeled 'ends.' The inner portion of the tube is then, carefully, extracted into a beaker labeled 'center.' This is the sample that will be used for wet sieving.

Wet sieving is done by selecting sieves of appropriate size, which is chosen to obtain the largest amount of sample in the smallest range of sizes. For example, if I had a medium-sized sand sample and was primarily homogenous, I would choose the 90 micron to 150 micron range. Three beakers are labeled > largest fraction (150 micron), target fraction (90-150 micron), and < smallest fraction (<90 micron). Wet sieving is done to obtain these target fractions, as well as remove any silts and clays. Sieve small amounts of sample at a time to make the process quicker. Once the samples are divided into the respective beakers, place the > largest fraction in the oven and the < smallest fraction in storage to let the fines settle (usually overnight). Once the > and < fractions are dry, they will be archived. Record the fractions used in the processing book and the date completed.

The target fraction beaker is placed under the fume hood and treated with HCl, which is used to remove carbonates. Prior to this treatment, you must have protective eyewear and gloves. Add enough HCl so there is approximately 1 cm on top of the

sample. Stir with a glass stir rod and record the results. Was there a reaction? If so, how intense (mild, moderate, strong)? If there was a reaction, let sit for 2 hours, decant HCl, and retreat. Repeat these steps until there is no reaction with the HCl and then let the sample sit overnight in the HCl. Prior to treating with bleach, the sample needs to be rinsed thoroughly. When bleach and HCl are combined, they form chlorine gas which is incredibly toxic. Therefore, the rule of thumb is that once the sample is 'clean' wash it 3 mores times. Washing is done with a carboy and a spray bottle of DI water. The carboy washes the sample about 3 times and the spray bottle is used to 'powerwash' (completed by tilting the beaker and migrating the stream of water from side to side as the sample moves from one side of the beaker to the other).

Once the target fraction has been rinsed thoroughly, the same procedure is completed using the bleach, which removes the organics from the sample. Once there is no reaction, the sample should sit in bleach overnight. The following day, the sample is rinsed thoroughly with DI water. At this point, the sample is ready to float.

To float the sample means to use polytungstate (at a specified density) so that the quartz and feldspars float and the heavy minerals sink. Prior to adding the polytungstate, the sample is divided into 4 test tubes (or as many as possible) and the remaining sample (if any) is archived. It must be labeled 'float' so the lab techs know which step the archived sample is prepared for. After sample is placed in 4 test tubes, they are placed in the sonicator for 10 minutes and then placed in the centrifuge for 10 minutes. This ensures that the individual grains have the opportunity to either float or sink. The test tubes are placed in a rack and then the bottom portion that has the heavy minerals is held

under liquid Nitrogen for 20-30 seconds until frozen. Using a spray bottle of DI, the quartz and feldspars are poured into a small beaker and placed in the oven to dry. Each step along the way should be recorded in the processing book. Treating the samples with HF removes the remaining fines from the sample, as well as etch the outside of the individual quartz grains to ensure proper age determination.

Appendix III—Blue Earth River OSL Sample Sites and Ages

Site ID	Easting	Northing	Height Above Channel (m)	Distance Upstream (m)	Age (yr BP_{2016})*	Σ (yr)
BEOSL1	410675	4874064	4.5	45572	**4.53****	**1.03**
BEOSL2	410442	4874523	4.4	44592	*12.00*	*2.17*
BEOSL3	410374	4875581	9.98	43024	*9.91*	*1.5*
BEOSL4	411705	4876651	2.59	37732	*5.18*	*0.94*
BEOSL5	412068	4876894	4.33	37340	**3.61**	**0.76**
BEOSL6	412924	4877101	10.36	35772	*9.7*	*2.45*
BEOSL7	413047	4877753	5.05	34792	**4.2**	**0.82**
BEOSL8	407699	4868190	10.28	61840	*32.5*	*7*
BEOSL9	408864	4868773	5.93	59684	*11.77*	*2.04*
BEOSL10	409784	4869715	2.87	55372	**3.3**	**0.67**
BEOSL11	409712	4872302	7.53	51452	**4.62**	**0.88**
BEOSL12	409647	4973612	1.53	47532	**1.57**	**0.45**
BEOSL13					**6.15**	**1.28**

*Years before present, where present = 2016

**Bolded ages represent high confidence. Ages in italics are suspected of partial bleaching and are thus likely too high.